times with DPBS. The medium was replaced with warm serum-free DMEM and rhodamine B-tagged polymers were added to a final concentration of 1.0 mg mL^{-1} for 30 min, before washing and measurement of calcein intensity by confocal microscopy and flow cytometry. As a control experiment, Lipofectin (final concentration: 10 μg mL^{-1}; Invitrogen) and Tween 20 (final concentration: 1.0 mg mL^{-1}, Aldrich) were used.

2.10. WST-8 assay

Assessment of the viability of cells after incubation with polymers for 24 h was carried out using a WST-8 assay (Dojindo, Tokyo, Japan), which is based on the cleavage of the tetrazolium salt to formazan by cellular mitochondrial dehydrogenase. Cells were seeded into 96-well plates at 1.0 × 10^4 cells/well in 100 μL of serum-containing DMEM. After preincubation for 3 h, polymers without fluorescence (10 μL) were added to the medium (final concentration: 1.0 mg mL^{-1}). Polymers in culture medium were incubated with cells for 21 h at 37 °C in 5% CO_2. Thereafter, 10 μL of WST-8 reagent was added to all cell culture medium and incubation was continued for a further 3 h (total 24 h). At the end of the incubation period, the microplates were read at 450 nm in an Appliskan microplate reader (ThermoFisher Scientific, MA, USA). A total of 110 μL of serum-containing DMEM with cells and 110 μL of serum-containing DMEM were used as the control and background, respectively. The average background absorbance from background control wells was subtracted from the sample data. The values for each sample were in the linear region of the standard curve of the WST-8 assay. Data are expressed as the means and SE (n = 8).

2.11. LDH release assay

Damage to cell membranes after incubation with polymers for 24 h was evaluated using a lactate dehydrogenase (LDH) assay kit (Wako, Osaka, Japan). Cells were seeded into 96-well plates at 1.0 × 10^4 cells/well in 100 μL of serum-containing DMEM. After preincubation for 3 h, polymers without fluorescence (10 μL) were added to the medium (final concentration: 1.0 mg mL^{-1}). Polymers in culture medium were incubated with cells for 24 h at 37 °C in 5% CO_2. Thereafter, 50 μL of cell-free supernatant was assayed using an LDH reagent kit according to the manufacturer's instructions. Absorbance at 560 nm was measured using an Appliskan microplate reader.

3. Results

We synthesized the rhoPMBs of approximately the same molecular weight but with different amphipathic natures, achieved by varying the MPC/BMA compositions (Table 1). The molar compositions determined by ^{1}H NMR (Fig. S1) approximately corresponded to their feed compositions. The rhoPMBs had hydrodynamic size of ca. 10 nm (Fig. S2). Importantly, zeta potential was nearly 0 mV. The fluorescence quantum yield of rhoPMB80 and rhoPMPC was slightly lower than that of rhoPMB30 and rhoPMB50 (Fig. S3); consequently, the fluorescence intensities of the former were compensated for during quantitative analysis. Covalent immobilization of rhodamine B on the polymers was confirmed by gel permeation chromatography (GPC) (Fig. S4). The GPC measurements also proved removal of the unreacted monomers and physically adsorbed dyes from the fluorescence-tagged polymers.

We used HepG2 (a human hepatocellular liver carcinoma cell line) cells because they are rich in mitochondria that can be easily visualized by confocal microscopy or studied by flow cytometry. In order to avoid potential artifacts caused by cell fixation, live cells were imaged under controlled temperature conditions. When rhoPMB30 was incubated with HepG2, it was observed to enter cells very rapidly and the fluorescence intensity continued to increase by real-time observation with confocal microscopy (Fig. 1a). Because endocytosis, including pinocytosis and phagocytosis, enables cells to internalize nanomaterials or small volumes of fluid that have no interaction with the plasma membrane into intracellular vesicles, we conducted internalization experiments in serum-free medium at 4 °C and under conditions of ATP depletion by incubating cells in 3.0 mM sodium azide and 50 mM 2-deoxy-D-glucose in DPBS at 37 °C. Under these conditions, active uptake by the cells is inhibited due to a deficiency in ATP. Surprisingly, substantial amount of rhoPMB30 was internalized even at 4 °C or in ATP depletion solution at 37 °C determined using confocal microscopy (Fig. 1b,c). We compared the fluorescence intensity of cells quantitatively using flow cytometry. The fluorescence intensity of cells incubated in ATP depletion solution reached the same level as that of cells in serum-free medium (Fig. 1d). A substantial level of fluorescence intensity compared with autofluorescence in cells incubated in serum-free medium at 4 °C was also confirmed. The observation that at least 50% of the uptake of rhoPMB30 into the cytosol occurred under conditions where endocytic processes were blocked suggests that the polymer is internalized in a non-endocytic manner. Interestingly, internalized rhoPMBs were able to escape from the cytoplasm when cells were incubated in polymer-free medium (Fig. S5). Although trends in polymer uptake and intracellular distribution were qualitatively similar in serum-free and serum-containing media, the comparable inhibition of cellular uptake of rhoPMB30 in serum-containing medium (Fig. 1d) presumably reflects binding to serum proteins [18]. Whether the fluorescent dyes located in the cytosol indicate the positions of rhoPMBs or simply fluorescent dye that has been enzymatically cleaved from the polymer was confirmed by relaxation modes of the fluorescent dyes in the cytosol using fluorescence correlation spectroscopy (FCS) [19]. FCS results showed slower translational diffusion of rhoPMB30 ($D_{rhoPMB30}$ = 30 μm^2/s) than from methacryloxyethyl thiocarbonyl rhodamine B (MTR, D_{MTR} = 220 μm^2/s) (Fig. 1e, Table 2). The results clearly indicate cytosolic entry of rhoPMB30 without cleavage of rhodamine B from the polymer. Further, we observed direct penetration of water-soluble rhoPMBs with higher weight-average molecular weight (M_w) of up to 4.0 × 10^5 (Table S1, Fig. S6). Thus, direct penetration of rhoPMBs is seemingly independent of their M_w.

The effects of MPC/BMA ratio (*i.e.*, amphipathicity) of rhoPMBs on direct penetration were investigated. Intense rhodamine B levels in the cytoplasm after incubation with rhoPMBs for 30 min were commonly observed under conditions where endocytic uptake was facilitated or blocked using confocal microscopy (Fig. 2a, b). Quantitative comparison by flow cytometry revealed that there was no clear relationship between the MPC/BMA ratios of the polymers and fluorescence intensities of stained cells (Fig. 2c) In contrast,

Table 1
Physical and chemical properties of the rhodamine B-tagged random copolymers used in this study.

Fluorescent polymers	MPC/BMA composition[a], mol/mol	M_N[b], kDa	M_W[b], kDa	Hydrodynamic size[c], nm (PI)	ζ-potential[d], mV	Fluorescence quantum yield
rhoPMB30	29/71	7.3	24.0	9.5 (0.275)	4.1 ± 2.1	0.625
rhoPMB50	45/55	9.2	29.0	10.0 (0.224)	4.5 ± 2.1	0.619
rhoPMB80	71/29	15.9	41.1	12.1 (0.206)	2.2 ± 3.6	0.491
rhoPMPC	MPC 100%	51.6	159	12.6 (0.635)	0.4 ± 2.1	0.462

[a] MPC; 2-methacryloyloxyethyl phosphorylcholine, BMA; *n*-butyl methacrylate. Determined from ^{1}H NMR.
[b] Number-average (M_N) and weight-average (M_w) molecular weights measured by gel permeation chromatography using poly(ethylene glycol) standards.
[c] Determined by dynamic light scattering in serum-free Dulbecco's modified Eagle's Medium (DMEM). The parentheses indicate polydispersity index (PI).
[d] Measured in serum-free DMEM.

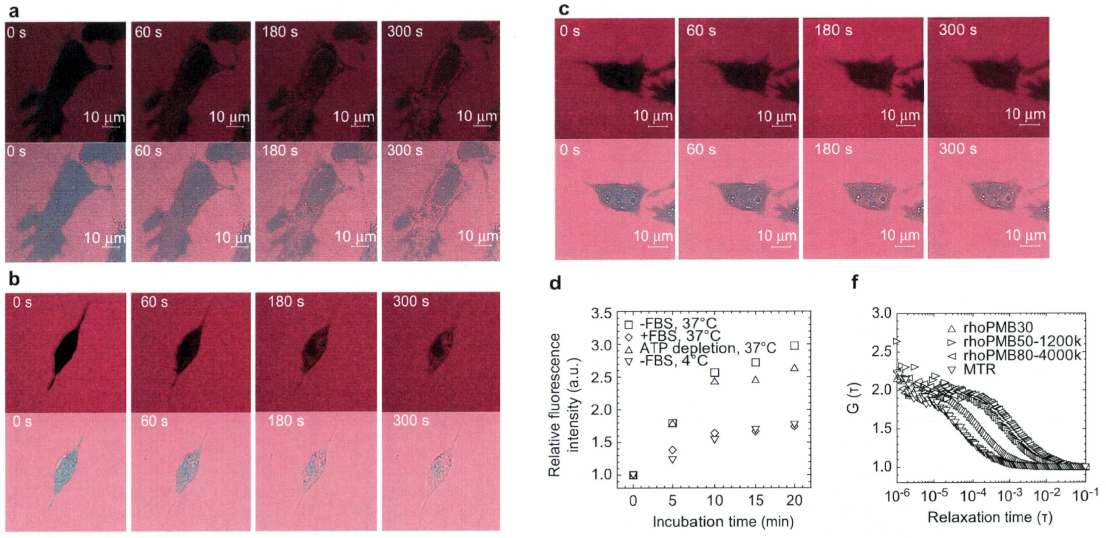

Fig. 1. Rhodamine B-tagged amphipathic phospholipid polymers exhibit direct penetration across the plasma membrane of live HepG2 cells. (a)–(c) Real-time rhodamine B (upper panels) and DIC/fluorescence merged (lower panels) confocal images of cells incubated with 1.0 mg mL^{-1} rhoPMB30 in serum-free medium at 37 °C (a), at 4 °C (b), or in ATP depletion solution at 37 °C (c). (d) Kinetics of internalization of rhoPMB30 (1.0 mg mL^{-1}) into cells in serum-free medium at 37 °C, at 4 °C, in serum-containing medium at 37 °C, or in ATP depletion solution at 37 °C. Rhodamine B fluorescence intensities of cells relative to autofluorescence intensities of untreated cells were quantified using flow cytometry (1.0×10^4 cells). (e) Low-power FCS curves for rhodamine B in the cytosol of cells incubated with rhoPMBs of different M_w or MTR at 25 °C.

Table 2
Summary of fluorescence correlation spectroscopy (FCS) results.

Samples	Diffusion time[b], μs	Diffusion coefficient, $\mu m^2/s$	Hydrodynamic radius, nm
rhoPMB30 in serum-free medium	220	45	4.9
rhoPMB30 in HepG2	330	30	7.3
rhoPMB50–1200k[a] in HepG2	760	13	17
rhoPMB80–4000k[a] in HepG2	1400	7.0	31
MTR in HepG2	46	220	1.0

[a] The M_w of rhoPMB50 (1200 kDa) and rhoPMB80 (4000 kDa) was obtained by gel permeation chromatography using poly(ethylene glycol) standards.
[b] Obtained by curve fitting of the autocorrelation function with a triplet state identified in the fitting, and two-dimensional fitting.

cells incubated with rhoPMPC (*i.e.*, MPC 100%) exhibited a low level of fluorescence intensity with statistically insignificant from the autofluorescence of untreated cells. Therefore, the polymer that completely lacks a hydrophobic BMA fails to pass across the plasma membrane. Next, we quantified the fluorescence intensity of cells after incubation with varying concentrations of rhoPMB30 because one of the characteristic features of amphiphilic polymers is the concentration dependence of polymeric aggregate formation in solution (Fig. 2d). The fluorescence intensity of cells apparently depended on concentration of rhoPMB30. Increased internalization amount of rhoPMB30 is in good agreement with decreased surface tension in the solution, which is caused by the aggregate formation. The rhoPMB30 was able to enter cells at more than 0.010 mg mL^{-1} and this concentration corresponded to the formation of hydrophobic domain of the polymer, which was determined by fluorescence spectroscopy using pyrene-tagged PMB [20] (Fig. S7). In contrast, the surface tension of rhoPMPC solution showing no cellular uptake remained unchanged (65–68 mN m^{-1}) throughout the concentration range. Therefore, we conclude that the direct penetration is amphiphaticity-dependent. Note that we found that internalization patterns of rhoPMBs in HeLa and HepG2 cells were observed to be similar (Fig. S8). The results indicate that direct penetration by rhoPMBs is not restricted to HepG2 cells and that it is probably a more general phenomenon.

The rhoPMB30 is enriched in the cytoplasm in tube-shaped compartments that are reminiscent of mitochondria. In order to identify the subcellular compartment in which rhoPMB30 is enriched, we stained cells with rhoPMB30 and MitoTracker Green FM. A high degree of colocalization of rhoPMB30 with MitoTracker in cytosol was observed using a confocal microscopy in multi-track mode (Fig. 3a). Because the obtained images were not caused by cross-talk between MitoTracker and rhodamine B (Fig. S9), rhoPMB30 was distributed in the mitochondria. The localization of rhoPMB30 is apparently attributed to the specificity of rhodamine B for mitochondria [21]. In order to determine the component that is responsible for its cytosolic localization we synthesized phospholipid analogous polymers that were covalently labeled with different fluorescent markers, namely, Hoechst 33258-tagged PMB30 (hoechstPMB30) and FITC-tagged PMB30 (fitcPMB30) (Table S2). Hoechst 33258 is a specific marker for nuclear DNA that forms a self-associated complex in the major groove of GC sequences in DNA [22]; FITC, in contrast, exhibits no organelle specificity. The hoechstPMB30 exhibited dominant nuclear localization (Fig. 3b). Confocal Z-section scanning images confirmed its localization at the nuclear membrane and throughout the entire nucleus (Fig. S10), indicating that hoechstPMB30 passes through both plasma and nuclear membranes. The fitcPMB30 was distributed throughout the cells probably due to non-specificity of FITC and PMB to organelles (Fig. 3c, Fig. S11). Hence, we conclude that the fluorescent tags determine the localization in the cytoplasm after direct penetration. Furthermore, simultaneous multiple-staining of mitochondria, nuclei, and the whole cytosol with rhoPMB30, hoechstPMB30, and fitcPMB30, respectively, was successful (Fig. 3d). The result indicates that the cytosolic distributions of these polymers are not mutually exclusive events. Although we demonstrated direct penetration using rhoPMBs, two coexisting mechanisms may still exist: energy-dependent and energy-independent. When cells were incubated with rhoPMB30 for 24 h, enhanced fluorescent contrast of vesicular structures and lower fluorescent intensity of mitochondria-localized rhoPMB30 was observed (Fig. S9). The energy-dependent portion of uptake would tend to imply an endocytic mechanism. In addition, it is reasonable to assume that there is increased interference due to enzymatic cleavage of rhoPMBs during prolonged incubation.

Finally, we tested whether translocation of rhoPMB30 is accompanied by the escape of cytosol-localized tracer dye. Cells were preloaded with calcein-AM which is trapped in the cytosol on conversion from a membrane-permeable to a membrane-impermeable form by intracellular esterases. The leakage of calcein in cells after incubation with 1.0 mg mL^{-1} of rhoPMB30 was quantified using flow cytometry. The calcein levels in cells treated with rhoPMB30 were not significantly different from those in untreated calcein-preloaded cells ($p = 0.18$, Fig. 4a). Confocal images revealed intracellular entry of rhoPMBs without any measurable leakage of calcein from the cells (Fig. S12). In contrast, the cells incubated with 10 μg ml^{-1} of Lipofectin or 1.0 mg mL^{-1} of Tween 20 showed statistically significant reductions in calcein levels [15% ($p = 0.06$) and 13% ($p = 0.09$), respectively] compared with untreated calcein-preloaded cells. Further, we measured acute cytotoxicity of cells using WST-8 and LDH release assays. The cells incubated with the PMBs survived at the same level as untreated control cells, whereas the cells incubated with Lipofectin or Tween 20 exhibited severe cytotoxicity (Fig. 4b,c).

4. Discussion

The underlying mechanism by which phospholipid analogous polymers pass through live cell membrane by non-endocytic processes remains unclear. Since rhoPMBs are electrically neutral, they do not create transient holes in the anionic plasma membrane. Earlier studies have shown energy-independent uptake using certain amphiphatic CPPs [18]. Apart from the pore-forming activities of amphipathic CPPs, the most attractive alternative explanations are either direct penetration into or across lipidic areas of the plasma membrane or facilitated diffusion. Helicity or sheet formation is not an essential structural requirement for peptides to cross biological membranes [23,24]. The concentration dependence of cellular uptake suggests direct penetration is enhanced by the formation of rhoPMBs aggregates. Direct penetration could involve the polymeric aggregates forming inverse micelle-like structures containing hydrophobic lipid cores, which eventually collapse back to form a more stable planar bilayer, thereby releasing the polymer into the cytosol. Another model envisages small-scale disruption of lipid packing in the surface membrane as a result of an interaction between the hydrophobic BMA and the membrane lipid core. Interestingly, nanoparticles in which the surface is coated with PMBs have been reported to impair both energy-dependent and energy-independent cellular uptake [25]. In this case, the BMA unit binds to the surface of the nanoparticles by hydrophobic interaction and becomes immobile. Thus, the outermost surface of the PMB-coated nanoparticles is completely covered with the zwitterionic phosphorylcholine headgroup that confer the property of biologically stealth on nanoparticles. These results imply that flexibility of the hydrophobic units of the polymer at the state of aggregate or free-

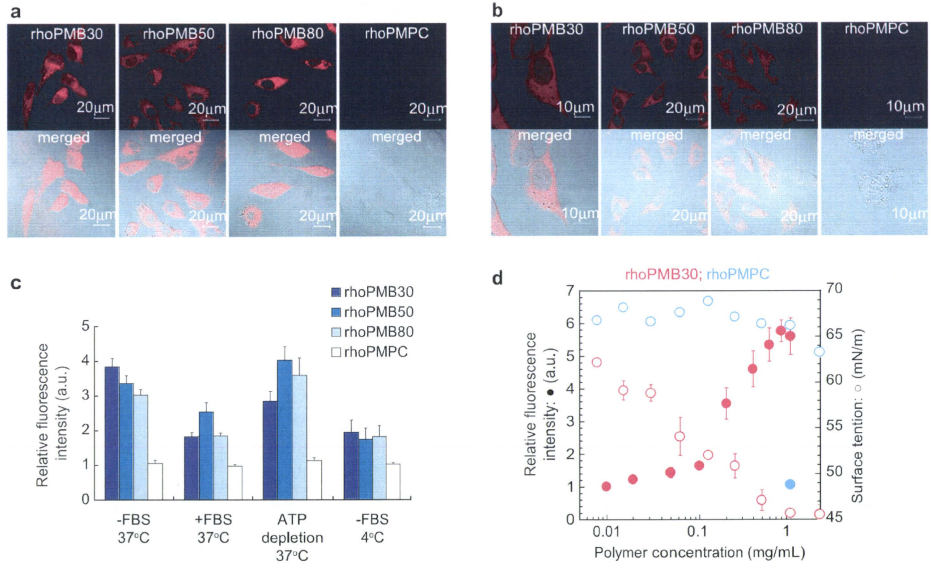

Fig. 2. Amphipathicity of the fluorescent polymers facilitates their direct penetration into live HepG2 cells. (a), (b) Confocal images of cells incubated with 1.0 mg mL^{-1} rhoPMB30, rhoPMB50, rhoPMB80, or rhoPMPC in serum-free medium for 30 min at 37 °C (a) or at 4 °C (b). All images were taken after rinsing the stained cells with DPBS. (c) Quantitative comparison of Rhodamine B fluorescence intensity of stained cells relative to the autofluorescence intensity of untreated control cells using flow cytometry (1.0×10^4 cells, the mean ± SD). Cells were incubated with the rhodamine B-tagged polymers (1.0 mg mL^{-1}) for 30 min in serum-free medium at 37 °C, in serum-containing medium at 37 °C, in ATP depletion solution at 37 °C, or in serum-free medium at 4 °C. (d) Relative fluorescence intensity of cells (open symbols) and surface tension in solution (filled symbols) as a function of rhoPMB30 (red) and rhoPMPC (blue) concentrations in serum-free medium. The surface tension was determined by the Wilhermy method. Data represent the mean ($n = 3$) ± SD.

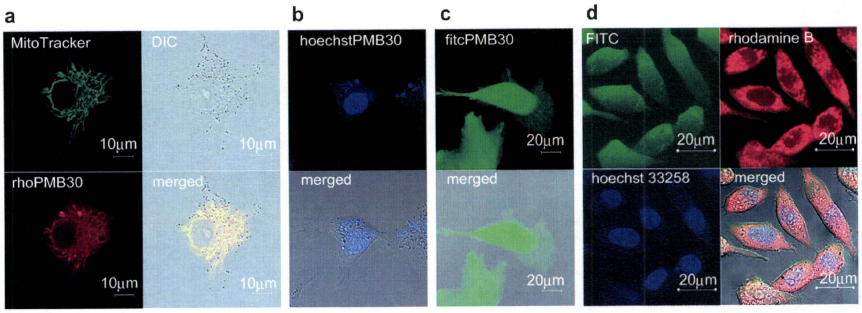

Fig. 3. Rhodamine B-, Hoechst 33258-, or FITC-tagged PMB30 distributes in subcellular compartments of live HepG2 based on the organelle specificity of the fluorescent dyes after direct penetration. (a) Confocal images of cells treated with 100 nM MitoTracker green FM and 1.0 mg mL^{-1} rhoPMB30 in serum-free medium at 37 °C using multi-track mode. (b), (c) Confocal images of cells treated with 1.0 mg mL^{-1} hoechstPMB30 (b) or fitcPMB30 (c) in serum-free medium for 30 min at 37 °C. (d) Confocal images of multiple color staining of live HepG2 cells incubated with rhoPMB30, hoechstPMB30, and fitcPMB30 (1 mg mL^{-1} each) in serum-free medium for 30 min at 37 °C. All images were taken after rinsing the stained cells with DPBS.

polymer is required for internalization across the lipidic cores of the plasma membrane.

Non-cytotoxic rapid cellular uptakes of cationic or amphipathic polymer vesicles comprising diblock copolymers of PMPC have recently been reported [26,27]. Internalization of these vesicles via unidentified mechanisms is suggested to be due to the favorable interactions of the biomimetic PMPC block, located in the corona of the polymersomes, with the cellular plasma membrane. The headgroups on the MPC unit are known to have a high degree of hydration, tenaciously binding around 15–25 or more water molecules per monomer unit [28–31]. At the same time, the hydration water molecules of the phospholipid polymers can exchange rapidly with other hydration or free water molecules [32–34]. This unique hydration, together with the overall neutral zwitterionic group of the MPC unit accounts for its superior non-cytotoxicity. Thus, in the present study, amphipathic rhoPMBs do not disrupt the integrity of the plasma membrane even at higher concentrations, allowing the formation of polymeric aggregates. We assume that the ability of both MPC units and natural phospholipids to form hydration shells enables these two types of molecule to readily fuse with each other. Amphipathicity-dependent direct penetration of nanomaterials has recently been achieved by coating gold nanoparticles with striations of alternating anionic and hydrophobic groups, forming a striped pattern at the molecular level [35]. It is likely that the exquisite arrangement of amphipathic domains on the nanoparticles permits non-disruptive fusion of the nanoparticle with cell membranes and subsequent penetration through the bilayer. In contrast, our phospholipid polymers which exhibit random arrangement of hydrophilic and hydrophobic groups directly penetrated across live cell membrane with subsequent access to the cytosol.

The amphiphaticity-dependent non-endocytic internalization by PMBs provides a new strategy about access of cargo molecules to the cytosol. Classically, the cellular internalization of hydrophilic macromolecules can only be achieved through the energy-dependent endocytic pathways [5,9]. In the past fifteen years several CPPs have been used successfully for the non-endocytic delivery and intracellular distribution of biomacromolecules across the plasma membrane of a wide variety of eukaryotic cells [10,11]. Translocation of active substances by transduction peptides have been utilized for diverse physiological and therapeutic applications, such as nuclear addressing [36], targeting to the central nerve system

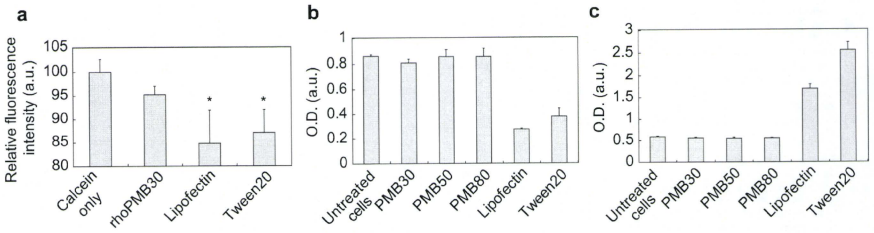

Fig. 4. Amphipathic rhoPMB30 generates no transient hole during its penetration across the plasma membrane of HepG2 cells. (a) Calcein intensity of cells after incubation with rhoPMB30 was determined using flow cytometry. Cells preliminarily incubated with 10 μM calcein-AM were treated with 1.0 mg mL^{-1} rhoPMB30 in serum-free medium for 30 min at 37 °C. Untreated cells and cells treated with 10 μg mL^{-1} Lipofectin or 1.0 mg mL^{-1} Tween 20 served as controls. Data represent the mean ($n = 3$) ± SD. The asterisks indicate statistically significant differences from cells with calcein only by Student's *t*-test ($p < 0.1$). (b), (c) Optical densities obtained from WST-8 (b) and LDH assays (c) after incubation of cells with the PMBs (1.0 mg mL^{-1}), Lipofectin (10 μg mL^{-1}), or Tween 20 (1 mg mL^{-1}) in serum-containing medium for 24 h at 37 °C. Data represent the mean ($n = 8$) ± SD.

across the blood–brain barrier [37], and identification of transcriptional targets [38]. Therefore, mechanism of direct penetration by the amphipathic polyphosphobetaines could be used to deliver nucleic acids, peptides, proteins, and other small molecules into the cytosol for therapeutic purpose. One of our next trials is to transport cargo molecules into cells or to tissues that are not normally easily accessible using PMBs.

5. Conclusions

Amphipathic phospholipid polymers bearing polar phosphorylcholine groups are capable of providing energy-independent rapid cellular uptake with targeted cytosolic localization, depending on the organelle specificity of the fluorescent tag. We attribute this non-cytotoxic direct penetration to the similar water structure in the hydration layer of the synthetic phospholipid polymers and natural phospholipids. The results may have relevance for live cell imaging and the delivery of therapeutic agents to specific sites within cells.

Acknowledgements

The author (T.G.) is grateful to the JSPS fellowship for providing partial financial support. We thank Dr. M. Takai, Dr. T. Konno, Dr. R. Matsuno, and Dr. M. Oba (The University of Tokyo) for discussion and helpful advice and Dr. R. Yoshida (The University of Tokyo) for provision of DLS apparatus.

Appendix

Figures with essential colour discrimination. Figs. 1–4 in this article may be difficult to interpret in black and white. The full colour images can be found in the on-line version, at doi:10.1016/j.biomaterials.2009.11.095.

Appendix. Supplementary data

The supplementary data associated with this article can be found in the on-line version at doi:10.1016/j.biomaterials.2009.11.095.

References

[1] Michalet X, Pinaud FF, Bentolila LA, Tsay JM, Doose S, Li JJ, et al. Quantum dots for live cells, in vivo imaging, and diagnostics. Science 2005;307:538–44.
[2] Ben NG, Adams SR, Ellisman MH, Tsien RY. The fluorescent toolbox for assessing protein location and function. Science 2006;312:217–24.
[3] Mornet S, Vasseur S, Grasset F, Duguet E. Magnetic nanoparticles design for medical diagnosis and therapy. J Mater Chem 2004;14:2161–75.
[4] Allen TM, Cullis PR. Drug delivery systems: entering the mainstream. Science 2004;303:1818–22.
[5] Boussif O, Lezoualc'h F, Zanta MA, Mergny MD, Scherman D, Demeneix B, et al. A versatile vector for gene and oligonucleotide transfer into cells in culture and in vivo: polyethylenimine. Proc Natl Acad Sci USA 1995;92:7297–301.
[6] Conner SD, Schmid SL. Regulated portals of entry into the cell. Nature 2003;422:37–44.
[7] Boas U, Heegaard PMH. Dendrimers in drug research. Chem Soc Rev 2004;33:43–63.
[8] Alivisatos AP, Gu WW, Larabell C. Quantum dots as cellular probes. Annu Rev Biomed Eng 2005;7:55–76.
[9] Kataoka K, Harada A, Nagasaki Y. Block copolymer micelles for drug delivery: design, characterization and biological significance. Adv Drug Deliv Rev 2001;47:113–31.
[10] Lindgren ME, Hällbrink MM, Elmquist AM, Langel U. Passage of cell-penetrating peptides across a human epithelial cell layer in vitro. Trends Pharmacol Sci 2000;21:99–103.
[11] Gupta B, Levchenko TS, Torchilin VP. Intracellular delivery of large molecules and small particles by cell-penetrating proteins and peptides. Adv Drug Deliv Rev 2005;57:637–51.
[12] Ishihara K, Iwasaki Y, Nakabayashi N. Polymeric lipid nanosphere consisting of water-soluble poly(2-methacryloyloxyethyl phosphorylcholine-co-n-butyl methacrylate). Polym J 1999;31:1231–6.
[13] Konno T, Watanabe J, Ishihara K. Enhanced solubility of paclitaxel using water-soluble and biocompatible 2-methacryloyloxyethyl phosphorylcholine polymers. J Biomed Mater Res A 2003;65:209–14.
[14] Wada M, Jinno H, Ueda M, Ikeda T, Kitajima M, Konno T, et al. Efficacy of an MPC-BMA co-polymer as a nanotransporter for paclitaxel. Anticancer Res 2007;27:1431–5.
[15] Miyata R, Ueda M, Jinno H, Konno T, Ishihara K, Ando N, et al. Selective targeting by preS1 domain of hepatitis B surface antigen conjugated with phosphorylcholine-based amphiphilic block copolymer micelles as a biocompatible, drug delivery carrier for treatment of human hepatocellular carcinoma with paclitaxel. Int J Cancer 2009;124:2460–7.
[16] Soma D, Kitayama J, Konno T, Ishihara K, Yamada J, Kamei T, et al. Intraperitoneal administration of paclitaxel solubilized with poly(2-methacryloxyethyl phosphorylcholine-co n-butyl methacrylate) for peritoneal dissemination of gastric cancer. Cancer Sci 2009;100:1979–85.
[17] Ishihara K, Ueda T, Nakabayashi N. Preparation of phospholipid polymers and their properties as hydrogel membrane. Polym J 1990;22:355–60.
[18] Oehlke J, Schellera A, Wiesnera B, Krausea E, Beyermanna M, Klauschenza E, et al. Cellular uptake of an α-helical amphiphilic model peptide with the potential to deliver polar compounds into the cell interior non-endocytically. Biochim Biophys Acta Biomembr 1998;1414:127–39.
[19] Lolin DL, Wiseman PW. Advances in image correlation spectroscopy: measuring number densities, aggregation states, and dynamics of fluorescently labeled macromolecules in cells. Cell Biochem Biophys 2007;49:141–64.
[20] Ham JS. A new electronic state in benzene. J Chem Phys 1953;21:756–8.
[21] Johnson LV, Walsh ML, Chen LB. Localization of mitochondria in living cells with rhodamine 123. Proc Natl Acad Sci USA 1980;77:990–4.
[22] Chiang S, Welch J, Rauscher FJ, Beerman TA. Effects of minor groove binding drugs on the interaction of TATA box binding protein and TFIIA with DNA. Biochemistry 1994;33:7033–40.
[23] Chaloin L, Vidal P, Heitz A, Van Mau N, Méry J, Divita G, et al. Conformations of primary amphiphilic carrier peptides in membrane mimicking environments. Biochemistry 1997;36:11179–87.
[24] Vivès E, Brodin P, Lebleu B. A truncated HIV-1 tat protein basic domain rapidly translocates through the plasma membrane and accumulates in the cell nucleus. J Biol Chem 1997;272:16010–7.
[25] Goto Y, Matsuno R, Konno T, Takai M, Ishihara K. Artificial cell membrane-covered nanoparticles embedding quantum dots as stable and highly sensitive fluorescence bioimaging probes. Biomacromolecules 2008;9:3252–7.
[26] Lomas H, Massignani M, Abdullah KA, Canton I, Lo Presti C, MacNeil S, et al. Non-cytotoxic polymer vesicles for rapid and efficient intracellular delivery. Faraday Discuss 2008;139:143–59.
[27] Madsen J, Armes SP, Bertal K, MacNeil S, Lewis AL. Preparation and aqueous solution properties of thermoresponsive biocompatible AB diblock copolymers. Biomacromolecules 2009;10:1875–87.
[28] Disalvo EA, Lairion F, Martini F, Almaleck H, Diaz S, Gordillo G. Water in biological membranes at interfaces: does it play a functional role? J Argent Chem Soc 2004;92:1–22.
[29] Yaseen M, Lu JR. The structure of zwitterionic phosphocholine surfactant monolayers. Langmuir 2006;22:5825–32.
[30] Nagle JF, Zhang R, Tristram-Nagle S, Sun W, Petrache HI, Suter RM. X-ray structure determination of fully hydrated L alpha phase dipalmitoylphosphatidylcholine bilayers. Biophys J 1996;70:1419–31.
[31] Morisaku T, Watanabe J, Konno T, Takai M, Ishihara K. Hydration of phosphorylcholine groups attached to highly swollen polymer hydrogels studied by thermal analysis. Polymer 2008;49:4652–7.
[32] Kitano H, Imai M, Mori T, Gemmei-Ide M, Yokoyama Y, Ishihara K. Structure of water in the vicinity of phospholipid analogue copolymers as studied by vibrational spectroscopy. Langmuir 2003;19:10260–6.
[33] Feng W, Nieh M-P, Zhu S, Brash JL, Harroun TA, Katsaras J. Characterization of biocompatible acrylate polymer brushes bearing oligo(ethylene glycol) and phosphorylcholine side chains in water by neutron reflectometry. Biointerphases 2007;2:34–43.
[34] Ishihara K, Nomura H, Mihara T, Kurita K, Iwasaki Y, Nakabayashi N. Why do phospholipid polymers reduce protein adsorption? J Biomed Mater Res 1998;39:323–30.
[35] Verma A, Uzun O, Hu Y, Hu Y, Han H-S, Watson N, et al. Surface-structure-regulated cell-membrane penetration by monolayer-protected nanoparticles. Nat Mater 2008;7:588–95.
[36] Jo D, Nashabi A, Doxsee C, Lin Q, Unutmaz D, Chen J, et al. Epigenetic regulation of gene structure and function with a cell-permeable Cre recombinase. Nat Biotechnol 2001;19:929–33.
[37] Schwarze SR, Ho A, Vocero-Akbani A, Dowdy SF. In vivo protein transduction: delivery of a biologically active protein into the mouse. Science 1999;285:1569–72.
[38] Mainguy G, Montesinos ML, Lesaffre B, Zevnik B, Karasawa M, Kothary R, et al. An induction gene trap for identifying a homeoprotein-regulated locus. Nat Biotechnol 2000;18:746–9.

Biomaterials 31 (2010) 6355–6362

Contents lists available at ScienceDirect

Biomaterials

journal homepage: www.elsevier.com/locate/biomaterials

2-Methacryloyloxyethyl phosphorylcholine polymer (MPC)-coating improves the transfection activity of GALA-modified lipid nanoparticles by assisting the cellular uptake and intracellular dissociation of plasmid DNA in primary hepatocytes

Masami Ukawa [a,1], Hidetaka Akita [a,1], Tomoya Masuda [a,1], Yasuhiro Hayashi [a], Tomohiro Konno [c], Kazuhiko Ishihara [b,c], Hideyoshi Harashima [a,*]

[a] Faculty of Pharmaceutical Sciences, Hokkaido University, Kita-12, Nishi-6, Kita-ku, Sapporo, Hokkaido 060-0812, Japan
[b] Department of Materials Engineering, School of Engineering, The University of Tokyo, 7-3-1 Hongo, Bunkyo-ku, Tokyo 113-8656, Japan
[c] Department of Bioengineering, School of Engineering, The University of Tokyo, 7-3-1 Hongo, Bunkyo-ku, Tokyo 113-8656, Japan

ARTICLE INFO

Article history:
Received 9 February 2010
Accepted 21 April 2010
Available online 27 May 2010

Keywords:
Isolated hepatocyte
Gene delivery
Intracellular trafficking
Endosomal escape
GALA
MPC polymer

ABSTRACT

We previously reported that modification of GALA peptide on the surface of liposomes enhanced fusion with endosomal membrane, and cytoplasmic release of encapsulated macromolecules. We report herein that an additional coating of GALA-modified liposomes with 2-methacryloyloxyethyl phosphorylcholine (MPC) polymer resulted in a two order of magnitude enhancement in the transfection activity of encapsulating plasmid DNA (pDNA). Quantification of the delivered gene copies in whole cells and isolated nuclei revealed that the increase of transfection activity can be attributed to improved efficiencies in cellular uptake and post-nuclear delivery processes. Imaging studies revealed that the intracellular dissociation of pDNA from the lipid envelope is enhanced by GALA modification and further coating with MPC polymer in a stepwise manner. The MPC polymer-coating decreased the ζ-potential of GALA-modified liposomes, suggesting that it assisted in the functional display of negatively charged GALA on the cationic liposomes by providing shielding from mutual electrostatic interactions. Collectively, these data indicate that MPC polymer-coating induced the fusogenic activity of the GALA-modified envelope with endosomes, leading to a more effective cytoplasmic release pDNA. The extensive fusion of the lipid envelope may also reduce electrostatic interactions between mRNA and cationic lipid components, thereby resulting in an enhancement in the translation process.

1. Introduction

The liver plays an important role in homeostasis and detoxification. Liver-targeting gene delivery represents a potentially promising strategy for curing a variety of intractable diseases. To date, numerous attempts have been made for the hepatic delivery of nucleic acids including short interference RNA (siRNA) and plasmid DNA (pDNA) by forming complexes with cationic liposomes (lipoplex) [1], polycations (polyplex) [2] and dendrimers [3]. In addition to these devices, encapsulating the molecular cargoes into a lipid envelope could protect them from clearance from the blood circulation and biological degradation. Successful examples of the in vivo use of lipid-encapsulation systems includes the tumor delivery of pDNA [4–6] and siRNA [7–9], in which the nucleic acids are encapsulated in a PEGylated liposome structure. The system is also applicable to the hepatic delivery of plasmid DNA [10] and siRNA [11].

From the pharmacokinetic point of view, a lipid envelope-type structure is also a potentially desirable system for controlling intracellular trafficking by overcoming biological membrane barriers such as the plasma/endosomal membrane and the nuclear membrane. It has been reported that envelope-type RNA viruses, such as the influenza virus, escapes from endosomes by fusion with the endosomal/lysosomal membrane, followed by the cytoplasmic release of its RNA genome. Of note, hemagglutinin (HA), which is present on the viral lipid envelopes plays a key role in membrane fusion via its conformational change in response to the acidic environment [12,13]. Inspired by the endosomal escape mechanism, the peptide derived from the N-terminus of the hemagglutinin subunit (HA-2) [14–16], or synthetic peptides (GALA) [17,18] were developed to induce endosomal escape, because it undergoes a structural change from a random coil to an α-helix under acidic

* Corresponding author. Tel.: +81 11 706 3919; fax: +81 11 706 4879.
E-mail address: harasima@pharm.hokudai.ac.jp (H. Harashima).
[1] Masami Ukawa, Hidetaka Akita and Tomoya Masuda equally contributed to this study.

0142-9612/$ – see front matter © 2010 Elsevier Ltd. All rights reserved.
doi:10.1016/j.biomaterials.2010.04.031

conditions. We previously reported on the development of a multifunctional envelope-type nano device (MEND) in which pDNA or siRNA is condensed with a polycation, followed by encapsulation by a lipid envelope [19]. The incorporation of cholesteryl GALA (chol-GALA) into the lipid envelope enhanced membrane fusion with the endosome, and thereby, increased the transfection activity and gene knockdown activity of the encapsulated pDNA [20] and siRNA [21–23], respectively.

For in vivo applications, non-toxicity is also an important issue that must be satisfied. Coating the surfaces of medical devices with 2-methacryloyloxyethyl phosphorylcholine (MPC) polymers suppresses biological reactions by inhibiting undesirable interactions with biomolecules and cells [24,25]. Furthermore, it was previously reported that the nanoparticles covered with the amphiphilic MPC polymer can avoid entrapment by macrophages [25]. A synthetic water-soluble polymer containing an MPC unit as a polar group and *n*-butyl methacrylate (BMA) group as a hydrophobic unit, poly(MPC-*co*-BMA)(PMB), forms nanoassembles or polymer aggregates in aqueous media. Thus, PMB could be useful as a therapeutic nanocarrier [26,27]. Meanwhile, the hydrophobic domains (BMAs) in PMB are also available for multivalent grafting (insertion) to the lipid layer. Thus, it is likely that PMB would be a suitable platform material for modifying the MPC unit on the surface of the lipid envelope of a MEND. We report herein that the in vitro transfection activity of a MEND is drastically increased by modification with GALA (GALA-MEND), and a further coating with PMB (MPC/GALA-MEND) in mouse primary hepatocytes. The intracellular trafficking of pDNA was compared among a MEND, a GALA-MEND and a GALA/MPC-MEND to clarify the mechanism related to this process.

2. Materials and methods

2.1. Materials

The reporter plasmid pcDNA3.1(+)-luc (7037 bp) encoding the firefly luciferase gene was purified with a Qiagen Endofree Plasmid Mega Kit (Qiagen GmbH, Hilden, Germany). Protamine sulfate salmon mint was purchased from Calbiochem (Darmstadt, Germany). 1,2-dioleyl-3-trimethylammonium propane (DOTAP), Cholesterol, and 2-Dioleoyl-*sn*-glycero-3-phosphoethanolamine-N-(7-nitro-2-1,3-benzoxadiazole-4-yl) (NBD-DOPE) were purchased from Avanti Polar Lipids, Inc. (Alabaster, AL, USA). Stearylated PEG lipids (STR-PEG_{2000}) and heparin sodium were purchased from Wako Pure Chemical Industries, Ltd. (Osaka, Japan). Cholesteryl-GALA was purchased from Kurabo Industries, Ltd. (Osaka, Japan). Hoechst 33342 was purchased from Dojindo Laboratories (Kumamoto, Japan). 2-Methacryloyloxyethyl phosphorylcholine (MPC) was obtained from NOF Co, Tokyo, Japan, which was synthesized using a previously reported method [28]. *n*-Butyl methacrylate (BMA) was purchased from Nacalai Tesque, Inc.(Kyoto, Japan). Methacryloxyethyl thiocarbamoyl rhodamine B (MTR) was purchased from Polysciences Inc. (Warrington, PA, USA). α, α′-Azobisisobutyronitrile (AIBN) was purchased from Kanto Chemical Co. Inc. (Tokyo, Japan). All other organic reagents and solvents were commercially available reagents of extra-pure grade and were used without further purification.

2.2. Synthesis of poly(MPC-*co*-BMA)(PMB50) and fluorescence PMB50

The water-soluble poly(MPC-*co*-BMA)(PMB50, The MPC unit mole fraction of which was 0.5) and rhodamine-labeled PMB50 (Rho-PMB50) were synthesized by a conventional radical polymerization technique using α,α′-azoisobutyronitrile (AIBN) as the initiator. The procedure used for the synthesis of Rho-PMB50 is summarized as follows: MPC (4.4 g), BMA (2.1 g), and MTR (20 mg) were placed in a glass ampoule, AIBN(82 mg) was dissolved in the mixture, and the solution was then diluted with ethanol to a concentration of 1 mol/L of monomer. Argon gas was bubbled into the solution for 5 min to eliminate oxygen, and the glass ampoule was then sealed. Polymerization was performed at 60 °C for a given time. After cooling the glass ampoule, the contents were poured into a large excess of a mixture of diethyl ether and chloroform (8/2 by volume) to eliminate the remaining monomer and precipitate the polymer. The precipitate was isolated on a glass-filter and dried *in vacuo*. The obtained polymers were dissolved in water, and the polymer solution was dialyzed against water using a Spectrapore membrane with a molecular weight cut-off of 3.5 kDa. Finally, the polymers were obtained as lyophilized powders. The composition in the PMB50 polymer was determined to be MPC/BMA = 0.46/0.54 by ^{1}H NMR(α-300, JEOL Co., Ltd., Tokyo, Japan) spectral measurements. The molecular weight of the polymers was measured by gel permeation chromatography (GPC, JASCO Co., Ltd., Tokyo, Japan). A mixture of methanol and water (7/3 by volume) containing 10 mmol/L of lithium bromide was used as the eluent for the GPC measurements, and well-defined poly(ethylene oxide) (PEO) was used as standard samples for the calibration curve.

2.3. Cell culture

Primary hepatocytes were collected from ICR mice 6 to 8 weeks of age. The mice were anesthetized with 200 μl of 10 mg/ml pentobarbital. Under anesthesia, a needle was introduced into the portal vein and perfused carried out using perfusion buffer (140 mM NaCl, 5.4 mM KCl, 0.50 mM NaH_2PO_4, 0.42 mM Na_2HPO_4, 4.2 mM $NaHCO_3$, 10 mM HEPES, 0.51 mM EDTA, 5.0 mM Glucose, pH 7.4) for 10 min, and subsequently collagenase buffer (140 mM NaCl, 5.4 mM KCl, 0.50 mM NaH_2PO_4, 0.42 mM Na_2HPO_4, 4.2 mM $NaHCO_3$, 10 mM HEPES, 6.7 mM $CaCl_2$, 0.5 mg/ml Collagenase, 0.05 mg/ml Trypsin inhibitor, pH 7.5) for 7 min. The liver was excised and the cells were suspended in DMEM. The suspension was filtered by 70 μm cell strainer (BD Falcon). The filtered suspension was centrifuged at 50 × g for 1 min at 4 °C, and the supernatant removed. The pellet was washed twice with DMEM, and suspended in culture medium (William's E medium with antibiotics, 10% serum, 1 nM insulin and 1 nM dexamethazone). An aliquot of the cell suspension was mixed with 0.3% trypan blue and the living cells and dead cells were counted. Cell viability was approximately 80%.

2.4. Preparation of MENDs

MENDs were prepared by the lipid hydration method as reported previously [29,30]. In a typical run, pDNA (0.1 mg/ml) was condensed with protamine (0.067 mg/ml) in 10 mM HEPES (pH 7.4), at a nitrogen/phosphate (N/P) ratio of 1.0. A lipid film was prepared in a glass test tube by evaporating a chloroform solution of the lipids, containing DOTAP, cholesterol and STR-PEG_{2000} (DOTAP/Cholesterol/STR-PEG_{2000} = 30:60:10, total lipid amount: 82.5 nmol). To prepare the GALA-MEND, 2 mol% chol-GALA was added to the lipid film composition. The prepared lipid film was then hydrated with the condensed DNA solution for 10 min at room temperature; the final lipid concentration was 0.55 mM. After hydration, to complete the lipid coating of the condensed DNA, the tube was sonicated for 1 min in a bath-type sonicator (AU-25C; Aiwa Co., Tokyo, Japan). To prepare the MPC/GALA-MEND, a PMB50 solution (0.2 w/v % of MEND solution) was added to the suspension to coat the envelope of the lipid-coated particles with PMB50, and the mixture was then incubated for 30 min at room temperature. The diameter and ζ-potential of the MEND were determined using an electrophoretic light-scattering spectrophotometer (Zetasizer; Malvern Instruments Ltd., Malvern, WR, UK).

2.5. Transfection and reporter gene assay

2×10^4 cells were seeded on a 24-well plate (Corning incorporated, Corning, NY, USA) in 500 μl of culture medium 1 day prior to transfection. The cells were incubated with a 250 μl aliquot of MEND solution in William's E medium with 10% serum without antibiotics (corresponding to 0.4 μg of DNA) for 3 h. The medium was then replaced with fresh medium containing 10% serum, and incubated for an additional 3 h. The cells were washed with 500 μl of phosphate-buffered saline (PBS) and lysed with 75 μl of reporter lysis buffer (Promega, Madison, WI, USA). Luciferase activity was initiated by the addition of 50 μl of luciferase assay reagent (Promega) to 20 μl of cell lysate, and was measured by means of a luminometer (Luminescencer-PSN; ATTO, Japan). The amount of protein in the cell lysate was determined using a BCA protein assay kit (PIERCE, Rockford, IL, USA).

2.6. Visualization of decoating and endosomal escape processes of the MENDs by confocal microscopy

To evaluate the decoating process of the MEND, 5×10^4 cells were seeded on a glass base dish (Iwaki, Osaka, Japan) in 2 ml of culture medium 1 day before transfection. To visualize the endosomal escape process of the MPC/GALA-MEND, the lipid envelope was further labeled with NBD by incorporating NBD-DOPE (1 mol % of total lipid). To analyze the intracellular trafficking of PMB50 labeled on the MPC/GALA-MEND, the PMB50 was partially replaced with Rho-PMB50 (20% of total PMB50). A 1 ml aliquot of the labeled MEND solution in William's E medium with 10% serum without antibiotics (corresponding to 2 μg of DNA) was incubated with the cells for 2 h. The medium was then replaced with fresh medium containing 10% serum and the cells were incubated for 4 h. To stain the nuclei, the cells were incubated with culture medium containing 5 μg/ml Hoechst 33342 for 10 min at room temperature. For labeling endosomes, the cells were incubated with culture medium containing 1 μg/ml Lysotracker Blue for 30 min at 37 °C, 5% CO_2. After washing the cells with 1 ml of observation buffer (135 mM NaCl, 5.4 mM KCl, 1.0 mM $MgCl_2$, 1.8 mM $CaCl_2$, 5.0 mM HEPES, 10 mM glucose, pH 7.3), the medium was changed to observation buffer and microscopic observation performed. Confocal images were obtained using a Zeiss LSM 510 META with an oil-immersion objective lens (Plan-Apochromat 63×/NA = 1.4).

To visualize the decoating process of the MEND, pDNA was labeled with rhodamine by means of the Label IT CX-rhodamine reagent (Mirus Corp., Madison, WI, USA) and packaged within the MEND. The lipid envelope of the MEND was further labeled with NBD by incorporating NBD-DOPE (1 mol% of total lipid). A 1 ml aliquot of labeled MEND solution in William's E medium with 10% serum without antibiotics (corresponding to 2 μg of DNA) was incubated with the cells for 2 h. The medium was then replaced with fresh medium containing 10% serum and the cells were incubated for a further 4 h. Staining with Hoechst 33342 and observation by confocal laser scanning microscopy were performed as described above.

2.7. Quantification of intracellular and nuclear-associated pDNA by real time PCR

1×10^5 cells were seeded on a 6-well plate in 2 ml of culture medium 1 day prior to transfection. The cells were incubated with a 1.25 ml aliquot of a MEND solution in William's E medium with 10% serum without antibiotics (corresponding to 2 μg of DNA) for 3 h. The medium was then replaced with fresh medium containing 10% serum and the cells were incubated for an additional 3 h. The cell surface-bound MENDs was then removed by washing 2 times with 1 ml of PBS containing heparin (20 units/ml) and the cells were collected by trypsinization (whole cell fraction). To quantify the nuclear pDNA, the fraction was further purified as described previously [29]. The collected cells were suspended in 375 μl of CellScrub Buffer (Gene Therapy Systems Inc.), and 125 μl of cell lysis solution (2% IGEPAL CA630, 40 mM NaCl, 12 mM $MgCl_2$, and 40 mM Tris–HCl, pH 7.4) was then added. The suspension was centrifuged at 9200 × g for 2 min at 4 °C, and the supernatant removed. This operation was repeated 3 times, and the obtained pellet was used as the nuclear fraction. DNA in the whole cell or nuclear fraction was extracted using a GenElute Mammalian Genomic DNA Miniprep Kit (Sigma) according to the manufacture's protocol, and subjected to real-time PCR with an ABI 7500 real-time system. The reaction mixture consisted of 5 μl of diluted sample DNA solution, 5 pmol of two types of primers (Luc (+): GGTCCTATGATTATGTCCGGTTATG and Luc(−): ATGTAGCCATCCATCCTTGTCAAT, or β-actin(+): AGAGGGAAATCGTGCGTGAC and β-actin(−): CAATAGTGATGACCTGGCCGT) and 12.5 μl of SYBR Green Realtime PCRMaster Mix (Toyobo, Osaka, Japan). The DNA was denaturized at 95 °C for 15 s, and annealing/extension was performed at 60 °C for 1 min. The denaturation/annealing cycle was repeated 40 times. The amount of pDNA was normalized by the number of nuclei quantified by the copy number of β-actin DNA.

3. Results

3.1. Physicochemical properties of MENDs and liposomes

The formation of DNA core particles and MEND particles was confirmed by their physicochemical properties, as measured by electrophoretic light-scattering spectrophotometer (Table 1). The initially prepared DNA core had a particle size of 100 nm and a ζ-potential of −35 mV at a charge ratio of 1. After coating the particle with a cationic lipid envelope that was free of GALA and MPC, the particle size increased to approximately 200 nm and the ζ-potential was inverted to +30 mV. This suggests that the DNA core was encapsulated by the lipid envelope. The incorporation of 2% GALA, a negatively charged peptide at physiological conditions decreased the ζ-potential to approximately +14 mV, whereas no significant difference in size was observed. This suggests that chol-GALA is incorporated in the lipid envelope, and thereby GALA peptide is displayed on the surface of the particle. Moreover, coating with the MPC polymer further decreased the ζ-potentials.

Table 1
Physicochemical properties of MPC/GALA-MEND.

	Size (nm)	ζ-potential (mV)	Polydispersity index
Condensed DNA	103 ± 8	−34.0 ± 9.5	0.13 ± 0.02
MEND	206 ± 23	29.1 ± 2.7	0.27 ± 0.03
GALA-MEND	167 ± 21	13.9 ± 1.4[a]	0.25 ± 0.02
MPC/GALA-MEND	190 ± 3	−1.63 ± 4.9[a,b]	0.22 ± 0.01

Data are presented as the mean ± SD for three independent experiments. Significant differences were determined by one-way analysis of variance (ANOVA), followed by Student-Newman-Keuls test.
[a] $P < 0.01$ against MEND.
[b] $P < 0.01$ against GALA-MEND.

The effect of the MPC polymer-coating on the physicochemical characteristics of liposomes was also investigated (Table 2). Without GALA-modification, the ζ-potential of the liposomes was comparable regardless of the MPC coating. In contrast, in the case of GALA-modification, the presence of the MPC polymer-coating decreased the ζ-potentials. Collectively, these data indicate that the MPC polymer-coating affects the ζ-potentials of nanoparticles only when GALA is present on the surface of the lipid envelope.

3.2. Comparison of transfection efficiency among MEND, GALA-MEND and MPC/GALA-MEND

The effect of GALA-modification and MPC polymer-coating on transfection efficiency was evaluated. MEND, GALA-MEND and MPC/GALA-MEND were prepared with luciferase (GL3)-encoding pDNA as a marker gene, and were transfected into mouse primary hepatocytes. At 6 h after the transfection, the expression level was low, and no significant differences in transgene expression were observed between the GALA-MEND and MPC/GALA-MEND (data not shown). In contrast, the transfection activity for particles modified with GALA and coated with the MPC polymer were markedly increased in a stepwise manner on a logarithmic scale at 24 h post-transfection. Of note, is the fact that the luciferase activity for the MPC/GALA-MEND was 100 times higher than that for the GALA-MEND (Fig. 1). Without modification with GALA, the transfection activity of MEND was not enhanced, even when it was coated with the MPC polymer (Supplemental Information Fig. 1), suggesting that the MPC polymer enhanced transgene expression by assisting the function of GALA.

3.3. Quantitative analysis of intracellular trafficking of MPC/GALA-MEND

Transfection activity is rate-limited by various intracellular barriers (i.e. cellular uptake, nuclear transfer). To clarify which of the intracellular processes was improved as the result of modification by GALA and the MPC polymer, pDNA extracted from whole cells or isolated nuclei was quantified by real-time PCR. Preliminary results showed that the amount of pDNA in the whole cell and nuclear fractions was dramatically decreased (approximately 1/20) at 24 h post-transfection compared with those measured at 6 h-post transfection, most likely due to the enzymatic degradation of pDNA. Thus, we evaluated the intracellular trafficking at 6 h-post transfection based on the assumption that intracellular trafficking at an early phase is a key determinant of the transfection activity at longer incubation times.

The cellular uptake of pDNA in GALA-MEND was decreased to 7.6% compared with MEND. However, its uptake activity was recovered in the case of the MPC/GALA-MEND (Fig. 2A). Although MPC polymer-modification increased cellular uptake, the extent (approximately 10-fold) is not sufficient to explain the two-orders of magnitude difference in transfection activity. Therefore, the MPC polymer may also affect other intracellular processes. To address this issue, the nuclear delivery of pDNA was quantified by nuclear

Table 2
Effect of MPC polymer-coating on ζ-potential of Liposome and GALA-Liposome.

ζ-potential (mV)		
	MPC polymer (−)	MPC polymer (+) (30 min)
Liposome	30.2 ± 3.1	32.9 ± 6.9
GALA-Liposome	24.8 ± 0.7	11.7 ± 3.5**

Data are presented as the mean ± SD for three independent experiments. Asterisks represent significant differences, as determined by analysis of variance (ANOVA) followed by the Student's *t*-test (**$p < 0.01$) against MPC polymer-uncoated group.

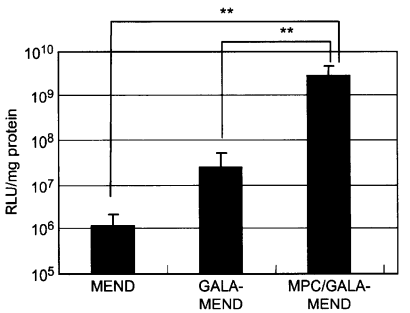

Fig. 1. Transfection efficiencies of MEND, GALA-MEND and MPC/GALA-MEND. Primary hepatocytes were incubated for 3 h with MEND, GALA-MEND and MPC/GALA-MEND. Luciferase activity was determined after a subsequent culture for 21 h in culture medium. The vertical axis shows luciferase activity expressed as relative light units (RLU) per milligram of protein (mg protein). Data are presented as the mean ± SD of three independent experiments. one-way analysis of variance (ANOVA), followed by Student-Newman-Keuls test (**; $P < 0.01$).

isolation, followed by real-time PCR (Fig. 2B). The nuclear transfer of pDNA varied nearly in parallel with cellular uptake, suggesting that the MPC polymer-coating has minor effect on the nuclear delivery process.

Finally, the transgene expression efficiency of nucleus-delivered pDNA (TE_{Nuc}), denoted as transfection activity divided by the amount of nucleus-delivered gene was compared (Fig. 2B). The TE_{Nuc} value for the GALA-MEND was 200-fold higher than that for MEND, and this value was further improved by 6.8-fold in the case of the MPC/GALA-MEND suggesting that the efficiency of post-nuclear transfer processes, including nuclear transcription and translation, was dramatically improved as the result of GALA-modification and further MPC polymer-coating (Fig. 2C).

3.4. Evaluation of endosomal escape of MPC/GALA-MEND

To address the mechanism for the improvement in nuclear delivery efficiency, the intracellular trafficking of MPC/GALA-MEND was analyzed by means of confocal laser scanning microscopy. The MPC/GALA-MEND, in which lipid envelope and PMB50 were labeled with NBD and rhodamine, respectively, was transfected, and the endosome/lysosome fraction was then stained with Lysotracker Blue at 6 h post-transfection. The signals derived from NBD-lipids and Lysotracker Blue were pseudocolored in green and red, respectively (Fig. 3A). The particles colocalized with (yellow clusters) and without (green clusters) colocalization with Lysotracker Blue are denoted as those in endosomes/lysosomes and those that escaped from endosome/lysosomes, respectively. As a result, the majority of the NBD signals (green) was observed in punctate form without colocalization with endosomes/lysosomes, suggesting that MPC/GALA-MEND escaped efficiently from the endosomes/lysosomes. In contrast to the significant degree of cytoplasmic distribution of lipid marker (Fig. 3A), Rho-PMB50 was predominantly colocalized with Lysotracker Blue (Fig. 3B). This indicates that PMB50 may be dissociated from the surface of the MEND sharing its fate with the outermost lipid envelope when it underwent endosomal escape.

3.5. Evaluation of intracellular dissociation of pDNA from MPC/GALA-MEND

We hypothesize that the presence of the MPC polymer facilitated the release of pDNA from the lipid envelope of the MEND. To investigate intracellular dissociation in cells, a double-labeled MEND was prepared, in which the pDNA was labeled with rhodamine and the lipid envelope was labeled with NBD (Fig. 4). In the case of the MEND, most of the pDNA signals were colocalized with the lipid envelope signals (Fig. 4A). In contrast, a significant portion of the pDNA signals was detected as non-co-localized forms in the GALA-MEND (Fig. 4B). Furthermore, the pDNA signals were predominantly red in the case of the MPC/GALA-MEND (Fig. 4C). Collectively, these data indicate that the intracellular dissociation of pDNA is enhanced in the order: MPC/GALA-MEND > GALA-MEND > MEND.

4. Discussion

In the present study, we propose a unique application of MPC polymers as a functional enhancer of peptides in which the surface of nanoparticles are modified, by controlling its topology. The MPC polymer-coating resulted in a drastic improvement in the

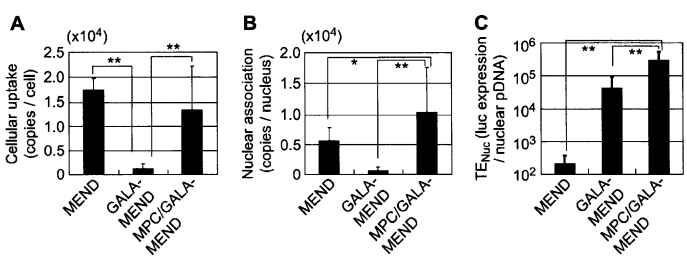

Fig. 2. Quantification of the amount of cellular and intranuclear pDNA after transfection of MENDs. Primary hepatocytes were incubated with the MEND, GALA-MEND and MPC/GALA-MEND for 3 h. After a subsequent culture for 3 h in culture medium, cell surface-bound MEND was removed by treatment with PBS containing heparin (20 units/ml). Thereafter, pDNA was extracted from whole cells or the nuclear fraction, and quantified by quantitative PCR. Cellular uptake (A) and nuclear pDNA (B) were calculated as the number of pDNA copies in whole cells and cell nuclei normalized by the copy number of b-actin genomic DNA in each fraction. Transgene expression efficiencies per nucleus-delivered pDNA were calculated as the luciferase activity divided by the number of nuclear pDNA (C). Data are presented as the mean ± SD of three independent experiments. one-way analysis of variance (ANOVA), followed by Student-Newman-Keuls test (*; $P < 0.05$, **; $P < 0.01$).

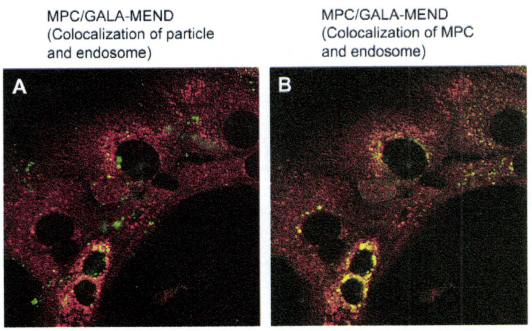

Fig. 3. Evaluation of the endosomal escape process of MPC/GALA-MEND by confocal microscopy analysis. (A) Cells were transfected with MPC/GALA-MEND incorporated with NBD-labeled lipids, and the endosome/lysosome fraction was then stained with Lysotracker Blue at 6 h post-transfection. The signals derived from NBD-lipids and Lysotracker Blue was pseudocolored in green and red, respectively. Particles that were colocalized with (yellow clusters) and without colocalization (green clusters) with Lysotracker Blue are denoted as those in endosomes/lysosomes and those that escaped from endosome/lysosomes, respectively. (B) Intracellular trafficking of the MPC polymer was also evaluated by visualizing a MPC/GALA-MEND prepared with Rho-PMB50. Signals derived from rhodamine and Lysotracker Blue were pseudocolored in green and red, respectively.

transfection activity of GALA-modified MEND by two-orders of magnitude. An analysis of intracellular trafficking revealed that the MPC polymer is a multifunctional device, and plays a key role in compensating and assisting the function of GALA-modified MEND in various processes.

First, the MPC polymer-coating improved the cellular uptake of GALA-MEND. It is generally accepted that electrostatic interactions between cationic particles and negatively charged heparin sulfate proteoglycans (HSPGs) on the cell membrane is a crucial driving force for cellular uptake [31,32]. Since GALA is a negatively charged peptide at physiological pH, its modification results in a decrease in the ζ-potential of a particle (Table 1), resulting in a reduction in cellular uptake (Fig. 1A). However, cellular uptake was unexpectedly recovered in the case of the MPC/GALA-MEND, even though the MPC polymer-coating further decreased the ζ-potential to a nearly neutral value (Table 1). Therefore, PMB50 may enhance cellular association via a unique mechanism except for electrostatic interactions. A very recent report showed that PMB50, and a series of derivatives efficiently enter the cytosol in living cells via the penetration of plasma membranes, even when energy-dependent endocytosis is blocked [33]. Although the mechanism of penetration remains to be clarified, the hydrophobic BMA units may efficiently interact with plasma membrane lipids. One of the model structures of MPC/GALA-MEND is illustrated in Fig. 5. Since the molecular weight of the PMB50 polymer used in the present study was high (Mn.;150,000), a portion of the hydrophobic BMA units would be incorporated into the lipid envelope of the MEND, and this would permit residual domains of PMB50 to be displayed on the surface of the particle. As a result, this structure permits particles to efficiently interact with the plasma membrane of cells via the strong affinity of the residual domain of PMB50 for the plasma membrane.

Another role of the MPC polymer is to assist the function of GALA in the endosomal fusion process. As shown in Fig. 3A, the MPC/GALA-MEND escapes from endosomes efficiently, while particles with PMB50 on the outermost envelope were trapped in endosomes/lysosomes (Fig. 3B). Furthermore, the majority of the pDNA was observed to be dissociated form from the lipid envelope in the case of modification with GALA (Fig. 4B) and the MPC polymer-coating (Fig. 4C), while pDNA was dominantly colocalized with

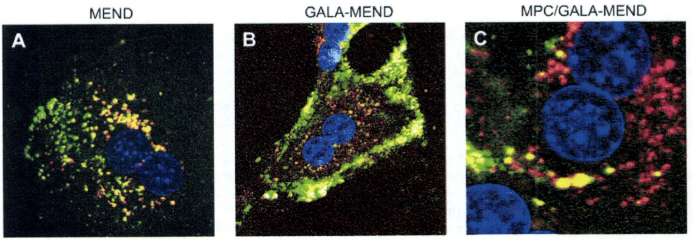

Fig. 4. Evaluation of the decoating process among MEND, GALA-MEND and MPC/GALA-MEND by confocal microscopy analysis. Primary hepatocytes were incubated with fluorescence-labeled MEND (A), GALA-MEND (B) and MPC/GALA-MEND (C), in which pDNA and the lipid envelope were labeled with rhodamine and NBD, respectively. Intracellular trafficking of the MPC/GALA-MEND was analyzed by means of confocal laser scanning microscopy. Red, green, blue signals indicate pDNA, lipid envelope of the MEND, and nuclei, respectively.

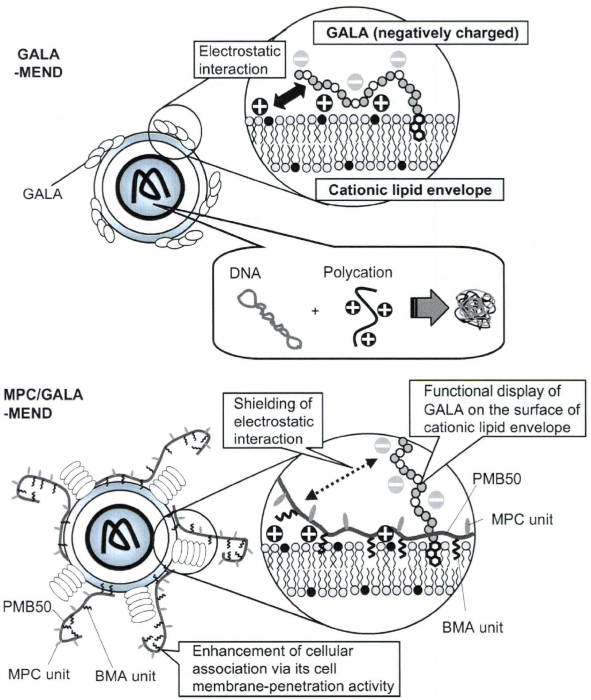

Fig. 5. Schematic diagram illustrating a possible structure of MPC/GALA-MEND. The GALA-MEND is coated with PMB50 polymer via the incorporation of hydrophobic BMA units into the lipid envelope. This permits the residual domains of PMB50 to be displayed on the surface of the particle. thereby allowing the particles to efficiently interact with the cellular surface via the membrane penetration activity of free PMB50 domain. Furthermore, coating with PMB50 leads to the formation of a thin hydrophilic MPC polymer layer just on the surface of the envelope, which blocks non-specific interactions between GALA and the cationic lipid envelope. This allows GALA to efficiently interaction with endosomes to trigger the membrane fusion.

the NBD-labeled lipid envelope (Fig. 4A) in the case of MEND. Collectively, these findings suggest that an MPC polymer-coating improves the fusogenic activity of the lipid envelope with endosomes by assisting the function of GALA, and thus the mechanism for endosomal escape shifts from a fusion-independent mode to a fusion-dependent one. Since the GALA peptide contains negatively charged amino acids, its function is partially prevented due to electrostatic interactions between GALA and the positively charged lipid envelope. The incorporation of PMB50 appears to lead to the formation of a thin hydrophilic MPC layer just on the surface of the envelope, which blocks non-specific interactions between GALA and the lipid envelope (Fig. 5). This hypothesis is supported by the physicochemical characteristics (ζ-potential) of the GALA-MEND and GALA-modified liposomes (Tables 1 and 2). Since the MPC units are amphoteric ions, PMB50 itself is a apparently neutral polymer. The presence of an MPC polymer-coating had no effect on the ζ-potential of GALA-unmodified cationic liposomes (Table 2). In contrast, the MPC polymer-coating significantly decreased the ζ-potential of liposomes that had been modified with GALA. Collectively, these data indicate that the presence of a hydrophilic MPC layer improved the surface display of GALA by preventing it from interacting with cationic liposomes.

The importance of the cytoplasmic dissociation process in the effective function of a cargo was also proposed in siRNA-loaded MEND [21]. Since MENDs prepared by the lipid hydration method have a multi-lamellar membrane structure [34], siRNA, when released into the cytosol, continues to be associated with the excess amount of lipid envelope even in the case of a GALA-modified MEND. Thus, modification with GALA is insufficient for improving the gene-knockdown effect of an siRNA-loaded MEND. Meanwhile modification of the protocol used in the hydration method to a single unilamellar vesicle (SUV)-fusion method resulted in a more efficient intracellular dissociation of siRNA and drastically improved gene-knockdown activity. Moreover, it was also demonstrated that the incorporation of short PEG-modified lipids (i.e. tetraethyleneglycol (TEG)-conjugated cholesterol) improved

the particle uniformity of MEND particle with a reduced particle size. As a result, the TEG-modified lipid particles had an enhanced transfection activity, as the result of improved intracellular dissociation [29].

One of the major questions is how pDNA enters the nucleus in non-dividing primary hepatocytes. Previous microinjection studies demonstrated that more than a 100-fold excess of pDNA is required to achieve transgene expression by cytoplasmic microinjection compared to that by nuclear microinjection, suggesting that less than 1% of the cytoplasm-microinjected plasmid DNA reaches the nucleus [35]. Moreover, transgene expression after cytoplasmic microinjection is severely diminished when mitosis is blocked in HeLa cells [30]. Therefore, it would be expected that the nuclear delivery of naked DNA would be essentially prevented in non-dividing primary hepatocyte. Nevertheless, high levels of transgene expression were achieved, even in the case of the MPC/GALA-MEND (Fig. 1) in which pDNA was dissociated from the lipid envelope in the cells. We previously reported that the expression efficiency of pDNA condensed with protamine increased depending on the nitrogen/phosphate (N/P) ratio after cytoplasmic microinjection. Thus, one of the mechanisms involves a delivery of pDNA to the nucleus in the form of a condensed particle with protamine after endosomal escape and dissociation from the envelope. Alternatively, pDNA could be delivered to the nucleus in the form of naked DNA. It was previously reported that the cytoplasmic translocation of pDNA may be driven by the insertion of specific sequences such as the SV40 enhancer region [36–38]. Since the region includes consensus sequences for various transcription factors (i.e. AP-1, AP-2 and NFκB), they may accelerate nuclear delivery when bound to a specific sequence of pDNA. Hepatocyte plays a key role in biosynthesis and metabolism, and thus the expression levels of many kind of genes are regulated under a wide variety of transcription factors. Hepatocytes may accept the nuclear delivery of pDNA more readily with the assistance of transcription factors rich in the cytosol compared with other type of cells.

Finally, the transgene expression efficiency of nuclear-delivered pDNA (TE_{Nuc}) revealed that the step-wise improvement in transfection activity is largely due to post-nuclear transfer processes (i.e. nuclear transcription and translation) (Fig. 2D). Based on the assumption that non-dividing primary hepatocytes only accept pDNA in the naked form or as particles condensed with protamine, it is plausible that pDNA is subject to the transcription comparably, regardless of the carriers present. Meanwhile, a previous study indicated that in vitro translation activity was drastically inhibited in the presence of cationic carriers most probably the result of electrostatic interactions between the cationic component in gene carriers and mRNA [39]. As discussed above, the intracellular dissociation efficiency of pDNA increased in GALA-MEND, and further in MPC/GALA-MEND in relation to the altered endosomal escape mechanism (from the fusion independent to the dependent mode). Thus, the cationic lipid envelope remaining in the cytosol would be expected to be lower in the GALA-MEND and even more lower in the MPC/GALA-MEND by extensive membrane fusion with endosomes. Collectively, the overall improvement in the post-nuclear delivery process in the GALA-MEND and MPC/GALA-MEND can be explained by an increase of translational efficiency, which is the result of less interactions between mRNA and the cationic lipid components in the cytoplasm, although the mechanism is unclear at present.

5. Conclusions

In summary, we describe the development of a MPC polymer-coated lipid nanoparticle as an efficient gene carrier for primary hepatocytes. The presence of an MPC polymer-coating assisted cellular uptake and the subsequent cytoplasmic dissociation of pDNA from the lipid envelope by assisting the endosome-fusogenic function of GALA. Considering the potent biocompatibility of MPC polymers, the MPC/GALA-MEND appears to be a highly potent carrier for a liver-targeting gene delivery system via systemic administration.

Acknowledgements

The authors thank Dr. Milton S. Feather for his helpful advice in writing the manuscript. This work was supported in part by Grants-in-Aid for Scientific Research (A) and Grant-in-Aid for Young Scientists (A) from the Ministry of Education, Culture, Sports, Science and Technology (MEXT) of Japan, and Special Coordination Funds for Promoting Science and Technology.

Appendix. Supplementary data

The supplementary data associated with this article can be found in the on-line version at doi:10.1016/j.biomaterials.2010.04.031.

References

[1] Fumoto S, Kawakami S, Ito Y, Shigeta K, Yamashita F, Hashida M. Enhanced hepatocyte-selective in vivo gene expression by stabilized galactosylated liposome/plasmid DNA complex using sodium chloride for complex formation. Mol Ther 2004;10:719–29.
[2] Rozema DB, Lewis DL, Wakefield DH, Wong SC, Klein JJ, Roesch PL, et al. Dynamic polyconjugates for targeted in vivo delivery of siRNA to hepatocytes. Proc Natl Acad Sci U S A 2007;104:12982–7.
[3] Kim KS, Lei Y, Stolz DB, Liu D. Bifunctional compounds for targeted hepatic gene delivery. Gene Ther 2007;14:704–8.
[4] Hatakeyama H, Akita H, Kogure K, Oishi M, Nagasaki Y, Kihira Y, et al. Development of a novel systemic gene delivery system for cancer therapy with a tumor-specific cleavable PEG-lipid. Gene Ther 2007;14:68–77.
[5] Heyes J, Palmer L, Chan K, Giesbrecht C, Jeffs L, MacLachlan I. Lipid encapsulation enables the effective systemic delivery of polyplex plasmid DNA. Mol Ther 2007;15:713–20.
[6] Jeffs LB, Palmer LR, Ambegia EG, Giesbrecht C, Ewanick S, MacLachlan I. A scalable, extrusion-free method for efficient liposomal encapsulation of plasmid DNA. Pharm Res 2005;22:362–72.
[7] Chen Y, Sen J, Bathula SR, Yang Q, Fittipaldi R, Huang L. Novel cationic lipid that delivers siRNA and enhances therapeutic effect in lung cancer cells. Mol Pharm 2009;6:696–705.
[8] Judge AD, Robbins M, Tavakoli I, Levi J, Hu L, Fronda A, et al. Confirming the RNAi-mediated mechanism of action of siRNA-based cancer therapeutics in mice. J Clin Invest 2009;119:661–73.
[9] Yagi N, Manabe I, Tottori T, Ishihara A, Ogata F, Kim JH, et al. A nanoparticle system specifically designed to deliver short interfering RNA inhibits tumor growth in vivo. Cancer Res 2009;69:6531–8.
[10] El-Sayed A, Masuda T, Khalil I, Akita H, Harashima H. Enhanced gene expression by a novel stearylated INF7 peptide derivative through fusion independent endosomal escape. J Contr Release 2009;138:160–7.
[11] Akinc A, Goldberg M, Qin J, Dorkin JR, Gamba-Vitalo C, Maier M, et al. Development of lipidoid-siRNA formulations for systemic delivery to the liver. Mol Ther 2009;17:872–9.
[12] Bentz J, Mittal A. Deployment of membrane fusion protein domains during fusion. Cell Biol Int 2000;24:819–38.
[13] Jardetzky TS, Lamb RA. Virology: a class act. Nature 2004;427:307–8.
[14] Plank C, Oberhauser B, Mechtler K, Koch C, Wagner E. The influence of endosome-disruptive peptides on gene transfer using synthetic virus-like gene transfer systems. J Biol Chem 1994;269:12918–24.
[15] Skehel JJ, Cross K, Steinhauer D, Wiley DC. Influenza fusion peptides. Biochem Soc Trans 2001;29:623–6.
[16] Wagner E. Effects of membrane-active agents in gene delivery. J Control Release 1998;53:155–8.
[17] Li W, Nicol F, Szoka Jr FC. GALA: a designed synthetic pH-responsive amphipathic peptide with applications in drug and gene delivery. Adv Drug Deliv Rev 2004;56:967–85.
[18] Parente RA, Nir S, Szoka Jr FC. Mechanism of leakage of phospholipid vesicle contents induced by the peptide GALA. Biochemistry 1990;29:8720–8.
[19] Kogure K, Akita H, Yamada Y, Harashima H. Multifunctional envelope-type nano device (MEND) as a non-viral gene delivery system. Adv Drug Deliv Rev 2008;60:559–71.
[20] Sasaki K, Kogure K, Chaki S, Nakamura Y, Moriguchi R, Hamada H, et al. An artificial virus-like nano carrier system: enhanced endosomal escape of nanoparticles via synergistic action of pH-sensitive fusogenic peptide derivatives. Anal Bioanal Chem 2008;391:2717–27.

[21] Akita H, Kogure K, Moriguchi R, Nakamura Y, Higashi T, Nakamura T, et al. Nanoparticles for ex vivo siRNA delivery to dendritoc cells for canner vaccine: Programmed endosomal escape and dissociation. J Contr Release 2010;143:311–7.
[22] Hatakeyama H, Ito E, Akita H, Oishi M, Nagasaki Y, Futaki S, et al. A pH-sensitive fusogenic peptide facilitates endosomal escape and greatly enhances the gene silencing of siRNA-containing nanoparticles in vitro and in vivo. J Contr Release 2009:139:127–32.
[23] Sakurai Y, Hatakeyama H, Akita H, Oishi M, Nagasaki Y, Futaki S, et al. Efficient short interference RNA delivery to tumor cells using a combination of octaarginine, GALA and tumor-specific, cleavable polyethylene glycol system. Biol Pharm Bull 2009;32:928–32.
[24] Ishihara K, Shinozuka T, Hanazaki Y, Iwasaki Y, Nakabayashi N. Improvement of blood compatibility on cellulose hemodialysis membrane: IV. Phospholipid polymer bonded to the membrane surface. J Biomater Sci Polym Ed 1999;10:271–82.
[25] Moro T, Takatori Y, Ishihara K, Konno T, Takigawa Y, Matsushita T, et al. Surface grafting of artificial joints with a biocompatible polymer for preventing periprosthetic osteolysis. Nat Mater 2004;3:829–36.
[26] Soma D, Kitayama J, Konno T, Ishihara K, Yamada J, Kamei T, et al. Intraperitoneal administration of paclitaxel solubilized with poly(2-methacryloxyethyl phosphorylcholine-co n-butyl methacrylate) for peritoneal dissemination of gastric cancer. Cancer Sci 2009;100:1979–85.
[27] Wada M, Jinno H, Ueda M, Ikeda T, Kitajima M, Konno T, et al. Efficacy of an MPC-BMA co-polymer as a nanotransporter for paclitaxel. Anticancer Res 2007;27:1431–5.
[28] Ishihara K, Ueda T, Nakabayashi N. Preparation of phospholipid polymers and their properties as polymer hydrogel membranes. Polym J 1990;22: 355–60.
[29] Masuda T, Akita H, Niikura K, Nishio T, Ukawa M, Enoto K, et al. Envelope-type lipid nanoparticles incorporating a short PEG-lipid conjugate for improved control of intracellular trafficking and transgene transcription. Biomaterials 2009;30:4806–14.
[30] Masuda T, Akita H, Nishio T, Niikura K, Kogure K, Ijiro K, et al. Development of lipid particles targeted via sugar-lipid conjugates as novel nuclear gene delivery system. Biomaterials 2008;29:709–23.
[31] Mislick KA, Baldeschwieler JD. Evidence for the role of proteoglycans in cation-mediated gene transfer. Proc Natl Acad Sci U S A 1996;93:12349–54.
[32] Mounkes LC, Zhong W, Cipres-Palacin G, Heath TD, Debs RJ. Proteoglycans mediate cationic liposome-DNA complex-based gene delivery in vitro and in vivo. J Biol Chem 1998;273:26164–70.
[33] Goda T, Goto Y, Ishihara K. Cell-penetrating macromolecules: Direct penetration of amphipathic phospholipid polymers across plasma membrane of living cells. Biomaterials 2010;31:2380–7.
[34] Akita H, Kudo A, Minoura A, Yamaguti M, Khalil IA, Moriguchi R, et al. Multilayered nanoparticles for penetrating the endosome and nuclear membrane via a step-wise membrane fusion process. Biomaterials 2009;30:2940–9.
[35] Pollard H, Remy JS, Loussouarn G, Demolombe S, Behr JP, Escande D. Polyethylenimine but not cationic lipids promotes transgene delivery to the nucleus in mammalian cells. J Biol Chem 1998;273:7507–11.
[36] Dean DA. Import of plasmid DNA into the nucleus is sequence specific. Exp Cell Res 1997;230:293–302.
[37] Vaughan EE, Dean DA. Intracellular trafficking of plasmids during transfection is mediated by microtubules. Mol Ther 2006;13:422–8.
[38] Wilson GL, Dean BS, Wang G, Dean DA. Nuclear import of plasmid DNA in digitonin-permeabilized cells requires both cytoplasmic factors and specific DNA sequences. J Biol Chem 1999;274:22025–32.
[39] Hama S, Akita H, Iida S, Mizuguchi H, Harashima H. Quantitative and mechanism-based investigation of post-nuclear delivery events between adenovirus and lipoplex. Nucleic Acids Res 2007;35:1533–43.

Biomaterials 31 (2010) 8839–8846

Contents lists available at ScienceDirect

Biomaterials

journal homepage: www.elsevier.com/locate/biomaterials

The biological performance of cell-containing phospholipid polymer hydrogels in bulk and microscale form

Yan Xu [a,b,*], Kihoon Jang [a,b], Tomohiro Konno [d], Kazuhiko Ishihara [c,d], Kazuma Mawatari [a,b,d], Takehiko Kitamori [a,b,d,*]

[a] Department of Applied Chemistry, School of Engineering, The University of Tokyo, 7-3-1, Hongo, Bunkyo, Tokyo 113-8656, Japan
[b] Core Research for Evolutional Science and Technology (CREST), Japan Science and Technology Agency (JST), 5 Sanban-cho, Chiyoda, Tokyo 102-0075, Japan
[c] Department of Materials Engineering, School of Engineering, The University of Tokyo, 7-3-1, Hongo, Bunkyo, Tokyo 113-8656, Japan
[d] Department of Bioengineering, School of Engineering, The University of Tokyo, 7-3-1, Hongo, Bunkyo, Tokyo 113-8656, Japan

ARTICLE INFO

Article history:
Received 15 July 2010
Accepted 30 July 2010
Available online 21 August 2010

Keywords:
2-Methacryloyloxyethyl phosphorylcholine (MPC)
Hydrogel
Microchip
Cell-based assays
Viability
Cytotoxicity

ABSTRACT

The biological performances of a cell-containing phospholipid polymer hydrogel in bulk and miniaturized formats without an additional culture medium support were investigated and compared. The cell-containing hydrogel was formed spontaneously when solutions of commercial polyvinyl alcohol (PVA) and the phospholipid polymer poly[2-methacryloyloxyethyl phosphorylcholine (MPC)-*co*-*n*-butyl methacrylate (BMA)-*co*-*p*-vinylphenylboronic acid (VPBA)] (PMBV) suspended with cells in a cell culture medium are mixed together. Bulk and miniaturized hydrogels, with approximate thicknesses of 3.1 mm and 400 μm, respectively, were prepared in a 96-well microplate and a glass microchip, respectively. In both cases, the hydrogels were homogeneous, and cells were spatially encapsulated. The long-term observation (4 and 8 days) of cell morphology suggested that cells were passively attached to the interface of the hydrogel but were unable to spread and flatten, which inhibited cell growth in both hydrogels. Viability evaluations revealed that cells in both hydrogel formats maintained the same high viability levels after long-term encapsulation. Cytotoxicity assays indicated that the cells in the miniaturized hydrogel maintained a high degree of correlation in cytotoxic sensitivity with the cells in the bulk hydrogel and a routine medium culture. The PMBV/PVA hydrogel not only provides a beneficial cytocompatible microenvironment for long-term cell survival without an additional culture medium support but also creates a static condition for cell sustainment in a microchip similar to that in bulk. The uniform long-term performances of PMBV/PVA hydrogels in bulk and miniaturized formats make them ideal for the development of long-term, flexible, three-dimensional, living cell-based tools for routine cell-based assays and applications on bulk to microscale levels.

1. Introduction

Hydrogels, cross-linked polymer networks that absorb large amounts of water, have attracted great interest in the biomaterial and biomedicine fields owing due to their favorable chemical, mechanical, interfacial, and mass transfer properties. Hydrogels incorporated with cells have been commonly employed in cell encapsulation and tissue engineering as encapsulation materials and tissue scaffolds because of their high cytocompatibility, three-dimensional (3D) tissue-like structures, and potential to form artificial extracellular matrices (ECMs) [1–3]. Due to developments in cell encapsulation and tissue engineering, recently, there has been an increasing trend toward the fabrication of cell-based tools with cell-containing hydrogels for cell-based applications such as toxin and drug screening, environmental monitoring, and sensing chemical and biological warfare agents [4–6]. In contrast to the two-dimensional (2D) substrates conventionally used in cell-based assays, hydrogels can provide an ideal 3D structural support for cells with ECM-like microenvironments consisting of complex cell-matrix and cell-soluble factor interactions, which may greatly improve the *in-vivo* relevance of cell-based assay results. Some cell-containing hydrogels have been developed and proven to spatially immobilize cells and finely engineer 3D microenvironments; these

* Corresponding authors. Department of Applied Chemistry, School of Engineering, The University of Tokyo, 7-3-1, Hongo, Bunkyo, Tokyo 113-8656, Japan. Tel.: +81 3 5841 7231; fax: +81 3 5841 6039.
E-mail addresses: xuyan@icl.t.u-tokyo.ac.jp (Y. Xu), kitamori@icl.t.u-tokyo.ac.jp (T. Kitamori).

0142-9612/$ – see front matter © 2010 Elsevier Ltd. All rights reserved.
doi:10.1016/j.biomaterials.2010.07.106

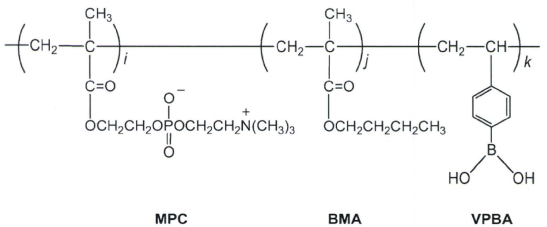

Fig. 1. Chemical structure of PMBV.

hydrogels have been used as 3D cell-based tools for research [4–6]. However, these cell-containing hydrogels can usually work only as living cell-based tools for a short time after cells are encapsulated in the hydrogels under very strict cell culture conditions with periodic changes of the fresh cell culture medium. In other words, these hydrogels exhibit poor performance for long-term cell sustainability, have low flexibility when applied to applications, and are therefore difficult to be commercialized and made portable. These limitations seriously impede their practical and widespread use in cell-based assays.

Recently, a phospholipid polymer hydrogel, composed of the newly designed poly[2-methacryloyloxyethyl phosphorylcholine (MPC)-*co*-*n*-butyl methacrylate (BMA)-*co*-*p*-vinylphenylboronic acid (VPBA)] (PMBV) (Fig. 1) and commercial polyvinyl alcohol (PVA), has been developed for reversible cell encapsulation [7,8]. Cells can be encapsulated in the hydrogel, which is spontaneously formed when the PMBV/cell suspension is mixed with the PVA solution in a cell culture medium (Fig. 2). We have previously detailed the synthesis and characterization of PMBV, emphasizing on the formation and properties of the PMBV/PVA hydrogel, and preliminarily evaluated cell behavior in the hydrogel in bulk [7] and in a microchip [8]. Our previous research implied that the PMBV/PVA hydrogel can possibly be used to fabricate long-term living cell-based tools and does not require the routine medium culture and the periodic medium change. This is a very intriguing development because the use of the PMBV/PVA hydrogel may bring great flexibility in cell-based assays and applications as it may overcome the aforementioned limitations of conventional cell-containing hydrogels when used as cell-based tools. Although the cells encapsulated in the PMBV/PVA hydrogel in bulk exhibit quite low proliferation over a period of several days [7], the long-term viability of cells in bulk hydrogels and its change with time are still unclear and need to be clarified. Therefore, to explore the possibility of using the PMBV/PVA hydrogel as a long-term cell-based tool, it is necessary to further investigate the long-term performance of cell sustainability for the PMBV/PVA hydrogel in bulk.

The microchip (or microfluidic chip) technology is a very promising technology for developing miniature and portable cell-based devices; this is believed to be the trend for future cell-based assays and applications [9–11]. In contrast to conventional devices such as cell culture dishes and microplates in which cells are cultured statically in bulk, microfluidic chip-based systems usually rely on continuous-perfusion dynamic cell culture for cell sustainment. In some continuous-perfusion microfluidic systems, cell behavior is quite different from that in the static culture in bulk, possibly leading to inconsistencies in cell-based assay results [12,13]. We speculate that the PMBV/PVA hydrogel may be a very useful support for guaranteeing uniform results of cell-based assays independent of devices, because the PMBV/PVA hydrogel provides a static condition for cell sustainment in a microchip similar to that in its bulk format. The high consistency between the PMBV/PVA hydrogel performances of the two formats is a precondition for the hydrogel to be practically applied in routine cell-based assays both in bulk and in a microchip. In our previous research, although the PMBV/PVA hydrogel exhibited a capability to encapsulate cells in a microchip [8], the performances of the hydrogel in a microchip and in bulk

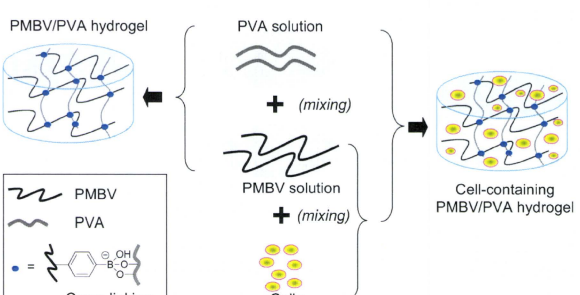

Fig. 2. Schematic diagram of PMBV/PVA hydrogel formation and fabrication of cell-containing PMBV/PVA hydrogel.

Table 1
Molecular properties of PMBV.

Abb.	Composition (mole fraction)[a]	Molecular weight (M_w)[b]	Solubility[c]		
	[MPC/BMA/VPBA]		H_2O	DMEM[d]	EBM-2[e]
PMBV	60/30/10	5.4×10^4	+	+	+

[a] Determined by ^1H NMR.
[b] Weight average molecular weight (M_w); determined by GPC, PEO standard.
[c] Evaluated by dissolving 1.0 mg polymer sample in a 1 mL solvent; +: soluble.
[d] DMEM: Dulbecco's modified Eagle's medium for culturing L929 cells.
[e] EBM-2: medium for culturing HAECs.

were not compared. To verify our speculation, it is necessary to investigate and compare the performances of the PMBV/PVA hydrogel in different formats when used in a cell-based assay.

In this study, we focused on investigating the long-term cell sustainability of the PMBV/PVA hydrogel in bulk formed in a 96-well microplate, which is a conventional and standard device widely used in various cell-based assays and applications; we further compared the performances of the bulk hydrogels with those of the miniaturized hydrogel formed in a microchip. By examining hydrogel formation, cell encapsulation, long-term cell viability, and cytotoxin assays, we explored the possibility of using the PMBV/PVA hydrogel as a general long-term living cell-based tool, compared the similarities and differences between the bulk and miniaturized hydrogels, and demonstrated the hydrogel's potential for use in cell-based applications. We believe that the information obtained from this study is important and meaningful in that it clarifies the optimal conditions for utilizing the PMBV/PVA hydrogel in cell-based assays from bulk to microscale levels, helps elucidating the inherent properties of the PMBV/PVA hydrogel and its mechanism for cell sustainability, and explores the possible applications of the PMBV/PVA hydrogel.

2. Materials and methods

2.1. Synthesis and characterization of PMBV

PMBV (Fig. 1) was synthesized by conventional radical polymerization according to the following process [7]. First, the desired amounts of MPC (synthesized as reported by us elsewhere [14]), BMA (Kanto Chemicals, Tokyo, Japan), VPBA (Tokyo Chemical Industry Co., Ltd., Tokyo, Japan) and α,α′-azobisisobutyronitrile (AIBN) (Kanto Chemicals) as the initiator were dissolved in ethanol in a glass ampoule; copolymerization was then performed at 60 °C for 6 h in the ampoule after it was sealed. The polymerization product was collected after reprecipitation from a diethyl ether/chloroform (8/2, v/v) solvent mixture. The remaining solvent was removed via vacuum drying to produce a white powder. The structure was identified by ^1H NMR (α-300; JEOL, Tokyo, Japan) spectra and Fourier transform infrared spectroscopy (FT-IR 615; JASCO, Tokyo, Japan). The average molecular weight was measured using a gel permeation chromatography (GPC) system (JASCO, Tokyo, Japan). The molecular properties of PMBV are summarized in Table 1.

2.2. Fabrication, setup, and operation of microchip

The microchip system for preparing the miniaturized PMBV/PVA hydrogel consists of a two-chamber chip, aluminum custom-made chip holder, Teflon™ capillaries, microtubes, and syringes equipped with a microsyringe pump (Fig. 3).

The two-chamber chip (Fig. 3) was fabricated by a photolithographic wet etching technique. Mechanically polished 0.7 mm-thick Pyrex glass substrates (7.0 cm × 3.0 cm) were used (top and bottom plates). While both channels and chambers (depth: 200 μm) were fabricated on the top plate, only chambers (depth: 200 μm) were fabricated on the bottom plate. Each plate fabrication was as follows. After inlet and outlet holes were drilled by ultrasonic sandblasting on the top plate, both top and bottom plates were annealed at 570 °C for 5 h. For good contact between the substrates and photoresist and to protect the substrates during glass etching, 20-nm-thick Cr and 100-nm-thick Au layers were sputtered on the bottom plate. A 2-μm-thick positive photoresist was spin-coated onto the Au metal layer and baked at 90 °C for 30 min. First, UV light was shone through a photomask to transfer the corresponding pattern onto the photoresist, which was then developed. Next, the Au and Cr layers were etched with I_2/NH_4I and $Ce(NH_4)_2(NO_3)_6$ solutions. The bare glass surface with the pattern was etched with a 50% HF solution at an etching rate of 13 μm/min. The remaining photoresist was then removed using acetone, and metals were removed in I_2/NH_4I and $Ce(NH_4)_2(NO_3)_6$ solutions. Finally, the fabricated top and bottom plates were bonded using a thermal bonding method.

The setup of the microchip system is shown in Fig. 3. The chip was first sandwiched within the holder. One head of the inlet capillary was connected to a Teflon™ screw using epoxy glue and then assembled to a target inlet of the chip with an o-ring; the other head was immersed in liquid in the microtube. For the outlet capillary, one head was connected to a Teflon™ nut using epoxy glue and then assembled to the syringe; the other was connected to a Teflon™ screw using epoxy glue and then assembled to a target outlet of the chip with an o-ring. The other inlets/outlets were sealed using Teflon™ screws with o-rings.

When introducing a solution to an objective chamber, the chip is positioned vertically by a chip holder so that all accessorial inlets/outlets lie on the upper side of the objective chamber (Fig. 3). By taking advantage of the chip design and operation, the liquid effluence from the outlet can be effectively avoided, and a fully filled chamber can be realized. The chip is positioned horizontally during the incubation process.

2.3. Preparation of cell suspensions

The mouse fibroblast cell line, L929 cells, and human arterial endothelial cells (HAECs) were used as model cells. L929 cells were routinely cultured in Dulbecco's modified Eagle's medium (DMEM) (Invitrogen, Grand Island, NY, USA) supplemented with 10% fetal bovine serum (FBS) (Sigma–Aldrich, St. Louis, MO, USA) using 60-mm cell culture dishes at 37 °C under 5% CO_2. After L929 cells became confluent, they were trypsinized and adjusted to a desired density with DMEM (supplemented with 10% FBS) containing 5.0 wt% of PMBV for the following experiments. HAECs were cultured according to a same protocol as used in the L929 cell culture. EBM-2 supplemented with EGM-2 SingleQuots (Cambrex Bio Science, Walkersville, MD, USA) was used as culture medium. The trypsinized HAECs were adjusted to a desired density with EBM-2 (supplemented with EGM-2 SingleQuots) containing 5.0 wt% of PMBV for the following experiments.

2.4. Encapsulation of cells in bulk and in the microchip

Cell encapsulation was performed in a standard 96-well microplate (Microtest™ 96, Becton Dickinson Labware) as a bulk sample and in the microchip (Fig. 3) as a miniaturized sample. Chips, holders, capillaries, and all other accessories were sterilized by autoclaving before use. All solutions were sterilized with 0.2-μm pore size sterilizing-grade filters before use.

Cell encapsulation in the microplate (i.e., in bulk). To encapsulate cells in a 96-well microplate, 25 μL of 2.5 wt% PVA (polymerization degree, about 1500; Wako, Osaka, Japan) solution (1× Dulbecco's phosphate buffered saline (D-PBS) as buffer) was first added to each well, after which 75 μL of cell suspension in a culture medium (L929: DMEM supplemented with 10% fetal bovine serum; HAECs: EBM-2 supplemented with EGM-2 SingleQuots) containing PMBV (5.0 wt%) was added. The microplate was immediately placed on a plate mixer (OPM-103, As One Corporation, Osaka, Japan) and shaken for 1 min at approximate 600 rpm. The cell-containing hydrogel formed in each well within several minutes. The microplate was then incubated at 37 °C in a cell culture incubator (Model MCO-17A1C; Sanyo).

Cell encapsulation in the microchip. The liquid operation in the microchip was conducted according to the process described in Section 2.2 and Fig. 3. To encapsulate cells in the microchip, 5 μL of 2.5 wt% PVA solution was first delivered into the chamber through the introducing microchannel using a microsyringe pump with a withdraw mode. Then, 15 μL of cell suspension in 5.0 wt% PMBV was introduced at a high flow rate of approximate 5 μL s^{-1}. The PMBV/PVA hydrogel spontaneously encapsulating the cells then formed in the chamber. With all inlets/outlets open, the chip was incubated at 37 °C in the cell culture incubator without any additional operation.

2.5. Evaluation of cell viability

The viabilities of the cells encapsulated in the hydrogels in both formats were investigated using live/dead assays (live/dead viability/cytotoxicity kit, Molecular Probes). Identical initial cell densities were applied in the two formats for comparison. For the bulk format formed in the 96-well microplate, after calcein-AM (2 μM)/ethidium homodimer-1 (4 μM) reagent mixture solution (50 μL) was added to each well holding 100 μL of cell-containing hydrogel, the microplate was incubated at room temperature for 45 min; it was then observed and analyzed using the fluorescence mode of an inverted microscope (IX 71; Olympus) with the CCD camera (Retiga EXi; QImaging). Great care was taken to minimize photobleaching due to excessive exposure. In a live/dead assay, green fluorescence (calcein, Ex/Em ~494 nm/~517 nm) is an indicator of live cells (live image), while red fluorescence (ethidium homodimer-1, Ex/Em ~528 nm/~617 nm) is an indicator of dead cells (dead image). The viability was estimated by counting the number of live and dead cells in more than three different areas of the well (i.e., more than three merged live/dead images) using the image processing program ImageJ 1.40g developed by the National Institutes of Health (NIH). The viability (or percentage of live cells) was defined as the *number of live cells/number of cells in total* (%). The viability of cells

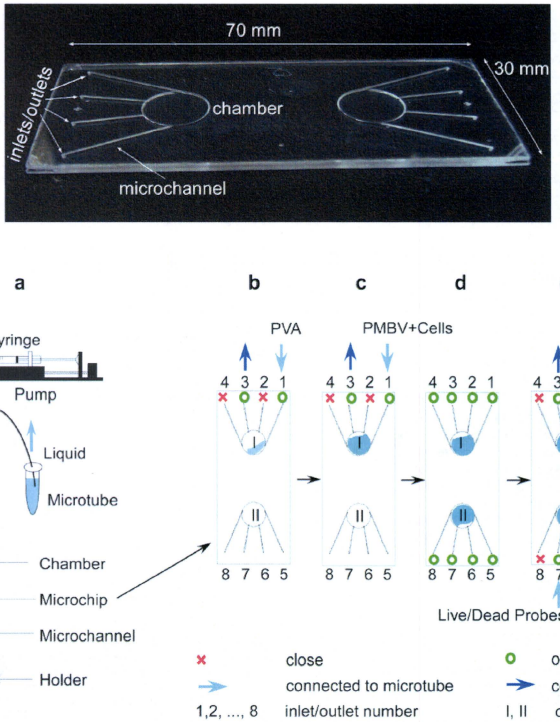

Fig. 3. (Top) Picture of two-chamber chip fabricated on glass substrates (70 mm × 30 mm) for preparing miniaturized cell-containing PMBV/PVA hydrogel. (Bottom) Setup and operation of two-chamber chip: (a) schematic diagram of system setup; (b) introduction of 5 μL PVA solution into Chamber I through inlet 1 and outlet 3; (c) introduction of 15 μL PMBV/cells suspension through the same inlet/outlet, immediately after which cell-containing PMBV/PVA hydrogel spontaneously forms in Chamber I, and cells are encapsulated in Chamber II through the same operation; (d) incubation of chip at 37 °C in cell culture incubator with all inlets/outlets open; and (e) introduction of 10 μL live/dead agents through inlet 2 and outlet 3 to Chamber I and through inlet 7 and outlet 6 to Chamber II, respectively, for viability assays, several days after encapsulation.

encapsulated in the hydrogel in the microchip was investigated using the same protocol. For each sample, 10 μL of the live/dead assay solution was introduced to the chip for the following viability assays.

2.6. Cell cytotoxicity analysis

After being encapsulated in the hydrogel for 4 days, L929 cells (initial density 1.0×10^6 mL^{-1}) were directly exposed to the toxin solutions. For the microplate containing 100 μL of cell-containing hydrogel in each well, 50 μL of toxin solution was added to each well. The microplate was then incubated in a cell culture incubator for 30 min at 37 °C. The supernatant in each well was removed post-exposure; 50 μL of the live/dead assay solution (2 μM calcein-AM/4 μM ethidium homodimer-1) was then added to each well. Following incubation at room temperature for 45 min, the labeled cells encapsulated in the hydrogel in the microplate were observed, and the percentage of dead cells (*number of dead cells/number of cells in total* (%)) was analyzed using fluorescence microscopy and the image processing program ImageJ. For the microchip, toxin screening experiments were performed according to a similar protocol as that used in the microplate experiments. Approximately 10 μL of toxin solution was injected into each chamber. After exposure, the solution remaining in the chip was drained using a syringe; approximately 10 μL of the live/dead assay solution was then injected into each chamber for the following viability assays.

3. Results and discussion

3.1. Hydrogel formation and cell encapsulation

In the PMBV/PVA hydrogel system, while PVA is a commercial water-soluble polymer, PMBV is a 2-methacryloyloxyethyl phosphorylcholine (MPC) containing polymer (i.e., MPC polymer). MPC polymers are well known for their high ability to suppress nonspecific protein adsorption and subsequent bioreactions [14–16]. The phosphorylcholine (PC) group in the MPC unit, which is a phospholipid polar group that also exists on the cell membrane, is believed to play a key role in the prevention of biofouling [17,18]. A series of MPC polymers have been developed for various conventional biomedical applications [19,20] and recent micro/nanotechnologies [21,22]. In this study, PMBV was synthesized by radical copolymerization of monomers of MPC, BMA, and VPBA (Table 1). PMBV is water-soluble due to its high composition of MPC units (60% mole fraction) [23], so it can be dissolved in various cell culture media (Table 1) and is easily

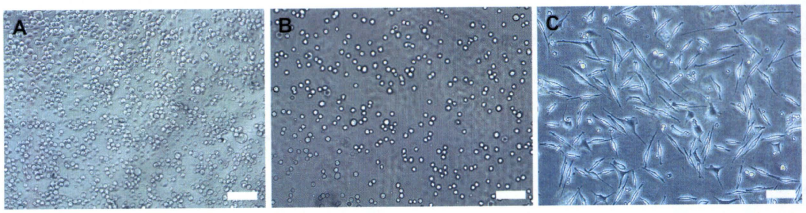

Fig. 4. Phase-contrast microscopic images of L929 cells (initial density = 1×10^6 mL^{-1}) after encapsulation (A) in bulk PMBV/PVA hydrogel formed in 96-well microplate and (B) in miniaturized PMBV/PVA hydrogel formed in microchip compared with (C) L929 cells routinely cultured in cell culture medium (DMEM) in cell culture dish. The scale bar is 100 μm.

handled in a microfluidic system. When PMBV and PVA aqueous solutions are mixed together, the PMBV/PVA hydrogel is formed spontaneously via a covalent cross-linking process between the phenylboronic acid groups of the VPBA units in PMBV and hydroxyl groups in PVA (Fig. 2). By mixing the PVA solution prepared in 1× PBS and the PMBV/cell suspension prepared in the culture medium, cells can be spontaneously encapsulated as the hydrogel forms (Fig. 2). The PMBV/PVA hydrogel dissociates to solutions when sugar solutions such as D-glucose and D-fructose are added, so the cell encapsulation with the PMBV/PVA hydrogel system is reversible. Since both the formation and dissociation of the cell-containing hydrogel occur under mild conditions without inflicting any adverse physical effects such as thermal and photo treatments, the PMBV/PVA hydrogel system is very advantageous for various routine cell-based applications.

Bulk and a miniaturized cell-containing PMBV/PVA hydrogels were prepared for comparison in a 96-well microplate and microchip, respectively, according to protocols with the same experimental conditions described in section 2. The 96-well microplate is a conventional and standard tool in analytical research and clinical diagnostic testing laboratories and is widely used in cell-based assays. The well of the 96-well microplate can be conveniently used to prepare hydrogels with thicknesses from several millimeters to 1 cm, i.e., a bulk-sized hydrogel. The microchip (Fig. 3), which is composed of two independent chambers and accessorial introducing channels, was fabricated on glass substrates (7.0 cm × 3.0 cm). Each chamber is 5.0 mm in radius, 400 μm in depth, and approximately 30 μL in total volume; the chip can be used to form a miniaturized hydrogel with sub-millimeter thickness, i.e., a micro-sized hydrogel. Accessorial introducing channels (700 μm in width and 200 μm in depth) to the chamber were designed to introduce liquids to/from the chambers. To make both hydrogel formats comparable, the optimal concentrations of the polymer solutions (i.e., 5.0 wt% PMBV and 2.5 wt% PVA) and an optimal mixing ratio (i.e., PMBV/PVA = 3/1, v/v) [7,8] were applied to prepare cell-containing hydrogels both in the microplate (bulk) and microchip (miniaturized). To facilitate sufficient mixing and homogeneous formation of the cell-containing hydrogel in the microplate, the microplate was shaken for 1 min at approximate 600 rpm with a microplate mixer immediately after adding the two solutions into the wells. Consequently, spatial encapsulation of cells was realized in the microchip hydrogel within several minutes (Fig. 4A). For cell encapsulation in the microchip, after a small volume (5 μL) of the PVA solution was introduced to the chamber, a large volume (15 μL) of PMBV/cells solution was introduced to the chamber at a high flow rate (approximate 5 μL s^{-1}). The small volume of the PVA solution in the chip was mixed sufficiently with the large volume of PMBV/cells solution when the two solutions collided in the chamber due to the introduction of the PMBV/cells solution at a high liquid rate in a very short time [24]. As a result, the cells were homogeneously and immediately encapsulated in the microchip hydrogel (Fig. 4B). In this research, a bulk-sized hydrogel with a millimeter-scale thickness of approximate 3.1 mm was prepared in each well of the microplate; in contrast, a miniaturized hydrogel with a microscale thickness of approximate 400 μm was prepared in the microchip chamber. The difference in dimension sizes (especially in the thickness) of the two hydrogels was obvious but comparable, which not only let them represent bulk-sized and micro-sized hydrogels, respectively, but also guaranteed the distribution of cells in the bulk to be as homogeneous as that in the microchip.

Fig. 4A and B demonstrate the morphology of L929 cells encapsulated in the microplate and microchip, respectively. In both cases, cells were round after encapsulation. The round shape of the cells was kept during the experiment taking place over several days (Fig. 5). In contrast, the L929 cells routinely cultured in DMEM in

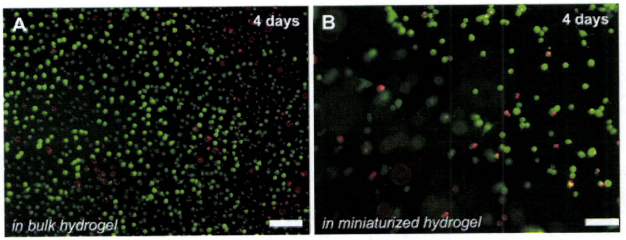

Fig. 5. Merged fluorescence images of live/dead assays of L929 cells (initial density = 1×10^6 mL^{-1}) after encapsulation for 4 days (A) in bulk PMBV/PVA hydrogel formed in 96-well microplate and (B) in miniaturized PMBV/PVA hydrogel formed in microchip. Green fluorescence indicates live cells, and red fluorescence indicates dead cells. The scale bar is 100 μm.

a cell culture dish tend to adhere, spread, and flatten to the surface and exhibit heterogeneous morphologies, as shown in Fig. 4C. The morphological difference between the cells encapsulated in the hydrogel and cells conventionally cultured in the culture dish suggests that cells encapsulated in the hydrogel are spatially confined in the hydrogel after encapsulation and may passively attach to the interface of the hydrogel but cannot spread and flatten whether in the microplate or microchip.

3.2. Long-term viability

Cell functions after encapsulation were investigated with two mammalian cell lines: L929 cells and HAECs. Both fibroblast cells (e.g., L929 cells) and endothelial cells (e.g., HAECs) are widely used as model cells in many cell biology applications, including cytotoxicity assays and tissue engineering. Cell-containing PMBV/PVA hydrogels with L929 cells and HAECs were prepared both in the microplate (bulk) and in the chip (miniaturized). For L929 cell encapsulation, an optimal high initial cell density of 1×10^6 mL^{-1} used in a preceding study [8] was applied in both format experiments. Fig. 5 demonstrates the representative fluorescence images for live/dead assays of L929 cells on the fourth day after encapsulation in the bulk and miniaturized hydrogel. In both hydrogel formats, only a few dead cells (indicated as red fluorescence) were found, indicating that most cells were live on the fourth day after encapsulation. Thus, almost equal calculated cell viabilities (4 days) of about 88.3% and 87.8% were obtained for the miniaturized and bulk hydrogels, respectively (Fig. 6). In other words, after 4 days, the viability of cells in the miniaturized hydrogel was highly uniform to that of cells in the bulk hydrogel. After 8 days, while the viability of L929 cells in the miniaturized hydrogel was as high as its viability on the fourth day, the viability of L929 cells in the bulk hydrogel decreased slightly to 73.5% (Fig. 6). Similarly, the 7-day viability of HAECs (initial density: 1.6×10^5 mL^{-1}) in the bulk hydrogel was also slightly lower than that in the miniaturized hydrogel (Fig. 7). This slight difference may simply result because the evaporation of water from bulk hydrogel in the microplate (as an open system) is faster than that from the miniaturized hydrogel in the microchip (as a semi-closed system); this does not appear to be an intrinsic property of the hydrogel. The evaporation leads to water loss from the hydrogel, which adversely changes the microenvironment of cells inside the hydrogel. To obtain reliable and comparative results, the following comparative investigations were therefore performed on the fourth day after encapsulation of cells in both hydrogel formats.

Although the mechanism of how the PMBV/PVA hydrogel supports cell survival is not yet completely clear, several considerations were addressed here. MPC polymers have been used to make hydrogels [25–27]. MPC polymer hydrogels are swollen in aqueous conditions and their gas permeability and solute permeability depend on their water contents. In general, MPC polymer hydrogels have high gas permeability [28] and solute permeability [29] because of their high water contents. MPC polymer hydrogels have also been reported to be suited to fabricating mimetic three-dimensional (3D) cell matrices for tissue engineering [26]; they benefit from their good biocompatibility in the physical entrapment of enzymes and soluble factors without deactivation [25] and high cytocompatibility for cell survival and gene expression [30,31]. As an MPC polymer hydrogel, the PMBV/PVA hydrogel is considered to have these common features. To keep a cell alive, nutrients for cell sustainment including various proteins, carbon sources, salts, and water are required. The PMBV/PVA hydrogel is composed of polymers and the cell culture medium. The medium containing these nutrients makes up more than 95 wt% of the hydrogel and supplies basic ingredients for cell maintenance in the hydrogel. Observations with a scanning electron microscope (SEM) showed that the lyophilized hydrogel has a porous structure with pore sizes of approximately 1 μm [7]. These micro-pores should facilitate the transport of these nutrients from the hydrogel to the cells and the permeation of the gas mixture (O_2 and CO_2) inside the hydrogel. For the microchip, all introducing channels of the microchip were designed to be relatively wide (700 μm) and deep (200 μm) so that gas transportation into the microchip is naturally favored. In contrast with the 96-well microplate, the microchip creates a semi-closed environment that effectively decreases the level of water

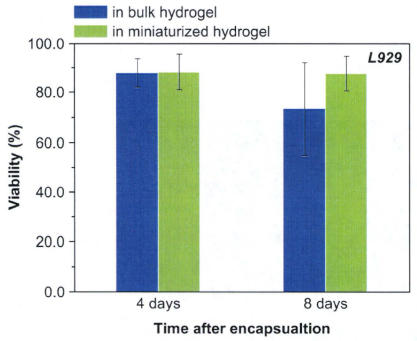

Fig. 6. Viabilities of L929 cells (initial density = 1×10^6 mL^{-1}) after encapsulation for 4 days and 8 days in bulk PMBV/PVA hydrogel formed in 96-well microplate compared with those in miniaturized PMBV/PVA hydrogel formed in microchip. Data are expressed as mean ± SD, $n > 3$.

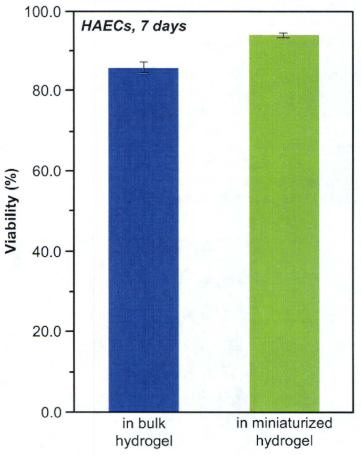

Fig. 7. Viabilities of HAECs (initial density = 1.6×10^5 mL^{-1}) after encapsulation for 7 days in bulk PMBV/PVA hydrogel formed in 96-well microplate compared with those in miniaturized PMBV/PVA hydrogel formed in microchip. Data are expressed as mean ± SD, $n > 3$.